S1. Supporting Information

This document contains Supporting Information for "*Direct linkage detection with multimodal IVA fusion reveals markers of age, sex, cognition, and schizophrenia in large neuroimaging studies*," by Rogers F. Silva, Eswar Damaraju, Xinhui Li, Peter Kochunov, Judith M. Ford, Daniel H. Mathalon, Jessica A. Turner, Theo G.M. van Erp, Tulay Adali, and Vince D. Calhoun.

S1.1. Image Acquisition Parameters

UK Biobank: **sMRI** T1-weighted structural MRI images were acquired using a 3D MPRAGE sequence at 1mm^3 isotropic sagittal slices with acquisition parameters: $208 \times 256 \times 256$ matrix, R=2, TI/TR=880/2000 ms. **rs-fMRI** Resting functional MRI were acquired axially at 2.4mm^3 resolution while the subjects fixated at a cross with the following acquisition parameters: $88 \times 88 \times 64$ matrix, TE/TR=39/735ms, MB=8, R=1, flip angle 52°. A pair of spin echo scans of opposite phase encoding direction in the same imaging resolution as rs-fMRI scans were acquired to estimate and correct distortions in rs-fMRI echo-planar images, and a single-band high resolution reference image was acquired at the start of the rs-fMRI scan to ensure good realignment and normalization. **dMRI** Diffusion MRI images were acquired using a standard Stejskal-Tanner spin-echo sequence at 2mm^3 isotropic resolution at three different b values (b = 0, 1000 and 2000 s/mm^2) and 50 distinct diffusion-encoding directions, each using a multi-band (MB) factor of 3.

COBRE: The COBRE dataset was collected using a 3-Tesla Siemens Tim Trio scanner (Qi et al., 2022). **sMRI** A high-resolution T1-weighted multi-echo MPRAGE (MEMPR) sequence was used with the following parameters (INDI, 2022)): TR/TE/TI = 2530/[1.64, 3.5, 5.36, 7.22, 9.08]/900 ms, flip angle = 7°, matrix = 256×256×176, voxel size = 1×1×1 mm^3, number of echos = 5, pixel bandwidth = 650 Hz, total scan time = 6 min. With 5 echoes, the TR, TI and time to encode partitions for the MEMPR are similar to that of a conventional MPRAGE, resulting in similar GM/WM/CSF contrast. MPRAGE: collected in the Sag plane - series interleaved - multi slice mode - single shot. **rs-fMRI** Rest data was collected with a standard single-shot, full k-space echo-planar imaging (EPI) sequence with ramp sampling correction, using the intercomissural line (AC-PC) as a reference and repetition time (TR)/echo time (TE) = 2,000/29 ms, voxel size = 3.75×3.75×4.55 mm^3, slice gap = 1.05 mm, 32 slices, flip angle = 75°, field of view (FOV) = 240×240 mm^2, matrix size = 64×64, and a total of 149 volumes. Slice Acquisition Order: collected in the Axial plane - series ascending - multi slice mode - interleaved. **dMRI** Diffusion data were acquired via a single-shot spin-echo echo planar imaging (EPI) with a twice-refocused balanced echo sequence to reduce eddy current distortions. The dMRI sequence included 30 directions, b = 800 s/mm^2 and five measurements of b = 0, for

6 minutes of acquisition time. The b = 0 measurements were interleaved after every six non-zero b-value measurements. The images were obtained in the axial direction along the AC-PC line. The FOV was 256×256 mm^2, 72 slices, 128×128 matrix, voxel size = 2×2×2 mm^3, TE = 84 ms, TR = 9000 ms, number of excitations (NEX) = 1, partial Fourier encoding of 3/4, and with a GRAPPA acceleration factor of 2 (Wu et al., 2015).

FBIRN: The fBIRN phase III dataset was collected from seven sites. Six of the seven sites used 3-Tesla Siemens Tim Trio scanners, and one site used a 3-Tesla General Electric (GE) Discovery MR750 scanner. **sMRI** A high-resolution Siemens MPRAGE sequence was acquired with the following parameters: TR/TE/TI = 2300/2.94/1100 ms, flip angle = 9°, matrix = 256×256×160. Likewise, a GE IR-SPGR sequence was acquired with the following parameters: TR/TE/TI = 5.95/1.99/45 ms, flip angle = 12°, matrix = 256×256×166. All scans covered the entire brain with FOV = 220 mm^2, voxel size = 0.86×0.86×1.2 mm^3, collected in the sagittal plane with GRAPPA/ASSET acceleration factor = 2, and NEX = 1 (Qi et al., 2022). **rs-fMRI** The same rs-fMRI parameters were used across all sites (Qi et al., 2022): a standard gradient EPI sequence, TR/TE = 2,000/30 ms, voxel size = 3.4375×3.4375×4 mm^3, slice gap = 1 mm, flip angle = 77°, FOV = 220×220 mm^2, and a total of 162 volumes. **dMRI** All acquisition parameters for all scanners were the same except for TE (Siemens 84ms/GE 81.7ms). The rest were as follows (Qi et al., 2018b): TR = 9000ms; matrix = 128×128; FOV = 256×256 mm^2; number of slices = 72; slice gap = 2 mm; voxel size 2×2×2 mm^3; flip angle = 90°; number of diffusion gradient directions = 30, b = 800 s/mm^2, 5 measurements with b = 0, NEX = 1. All images were registered to the first b = 0 image by FMRIB Linear Image Registration Tool (FLIRT).

MPRC: The MPRC dataset was collected in 3 sites, each with a different 3-Tesla Siemens scanner, using a standard EPI sequence. **sMRI** T1-weighted 3D MPRAGE collected in the saggital plane, 1×1×1mm^3. Siemens Allegra: TE/TR/TI=4.3/2500/1000ms, flip angle=8°. Siemens Trio: TE/TR/TI=2.9/2300/900ms, flip angle=9° (Schijven et al., 2023). **rs-fMRI** Siemens 3-Tesla Siemens Allegra scanner (TR/TE = 2,000/27 ms, voxel size = 3.44×3.44×4 mm^3, FOV = 220×220 mm^2, and 150 volumes); 3-Tesla Siemens Trio scanner (TR/TE = 2,210/30 ms, voxel size = 3.44×3.44×4 mm^3, FOV = 220×220 mm^2, and 140 volumes); and 3-Tesla Siemens Tim Trio scanner (TR/TE = 2,000/30 ms, voxel size = 1.72×1.72×4 mm^3, FOV = 220×220 mm^2, and 444 volumes) (Qi et al., 2022). **dMRI** All dMRI was performed using the Siemens 3T Trio scanner with a 32 channel phase array head coil. The high-angular resolution diffusion imaging (HARDI) protocol was used to assess white matter integrity as measured by fractional anisotropy (FA) (Wang et al., 2016; Wright et al., 2015). The dMRI data were collected using a single-shot, echo-planar, single refocusing spin-echo,

T2-weighted sequence, with GRAPPA (acceleration factor 2), yielding voxel dimensions 1.7×1.7×3.0 mm^3, acquisition time approximately 8 min. The sequence parameters were: TE/TR = 87/8,000 ms, FOV = 200 mm, axial slice orientation with 50 slices and no gap, 5 b = 0 images and 64 isotropically distributed diffusion-weighted directions with b = 700 s/mm^2. All data passed quality-assurance control of less than 3 mm accumulated motion during the scan. (Herskovits et al., 2015)

BSNIP: Subjects were scanned at six sites (Giakoumatos et al., 2015): Boston, MA (3.0 T, GE Signa); Detroit, MI (3.0 T, Siemens Allegra); Baltimore, MD (3.0 T, Siemens Trio Tim); Hartford, CT (3.0 T, Siemens Allegra); Dallas, TX (3.0 T, Philips Achieva); and Chicago, IL (3.0 T, GE Signa). This work only included data from Hartford and Baltimore sites. **sMRI** High-resolution isotropic T1-weighted MPRAGE scans (TR = 6.7 ms, TE = 3.1 ms, 8° flip angle, 256×240 matrix size, total scan duration ≈ 11 min, 170 sagittal slices, 1 mm slice thickness, 1×1×1.2 mm^3 voxel size) were acquired following the Alzheimer's Disease Neuroimaging Initiative (ADNI) protocol (http://www.loni.ucla.edu/ADNI) (Giakoumatos et al., 2015). **rs-fMRI** See Table S1 (Qi et al., 2022). **dMRI** Hartford used 32 gradient directions with b=1000 s/mm^2, one baseline scan with b=0 s/mm^2; TE = 85; TR = 6300 ms; FOV = 222 mm; a voxel size of 1.73×1.73×3 mm^3. Baltimore used 30 gradient directions with b=1000 s/mm^2, one baseline scan with b=0 s/mm^2; TE = 92 ms; TR = 6700 ms; FOV = 230 mm; a voxel size of 1.83×1.83×3 mm^3 (Cetin-Karayumak et al., 2020).

Table S1: **BSNIP Acquisition Parameters for rs-fMRI**.

Site	TR ms	TE ms	Flip angle	Slices	Voxel Size (mm^3)	Time points
Baltimore	2210	30	70°	36	3.4×3.4×4	140
Hartford	1500	27	70°	29	3.4×3.4×5	210

S1.2. UK Biobank Phenotype Variables

54 UK Biobank phenotype variables were further reduced to 26 variables for MANCOVA analysis and effect size analysis, as described below.

28 physical exercise variables were decomposed to 8 principal components by PCA. 2 age-related variables ("years since first sexual intercourse" and "years since started wearing glasses") were dropped because they are highly correlated with other age variables. 2 variables associated with fluid intelligence ("number of fluid intelligence questions attempted within time limit" and "interaction between number of attempts and score") and 4 other log variables ("time to complete round", "log time to answer", "inverse log duration screen displayed", "inverse log number of attempts") were also removed, resulting in 26 variables in total.

Table S2: **54 UK Biobank Phenotype Variables.**

Variable ID	Variable Name
f399 2 2	number of incorrect matches in round
f400 2 2	time to complete round
f699 2 0	length of time at current address
f864 2 0	number of daysweek walked 10 minutes
f874 2 0	duration of walks
f884 2 0	number of daysweek of moderate physical activity 10 minutes
f894 2 0	duration of moderate activity
f904 2 0	number of daysweek of vigorous physical activity 10 minutes
f914 2 0	duration of vigorous activity
f943 2 0	frequency of stair climbing in last 4 weeks
f971 2 0	frequency of walking for pleasure in last 4 weeks
f981 2 0	duration walking for pleasure
f991 2 0	frequency of strenuous sports in last 4 weeks
f1001 2 0	duration of strenuous sports
f1011 2 0	frequency of light diy in last 4 weeks
f1021 2 0	duration of light diy
f1050 2 0	time spend outdoors in summer
f1060 2 0	time spent outdoors in winter
f1070 2 0	time spent watching television tv
f1080 2 0	time spent using computer
f1160 2 0	sleep duration
f1438 2 0	bread intake
f1488 2 0	tea intake
f1498 2 0	coffee intake
f1558 2 0	alcohol intake frequency
f2139 2 0	age first had sexual intercourse
f2217 2 0	age started wearing glasses or contact lenses
f2624 2 0	frequency of heavy diy in last 4 weeks
f2634 2 0	duration of heavy diy
f3637 2 0	frequency of other exercises in last 4 weeks
f3647 2 0	duration of other exercises
f4288 2 0	time to answer
f4609 2 0	longest period of depression
f20016 2 0	fluid intelligence score
f20023 2 0	mean time to correctly identify matches
f20128 2 0	number of fluid intelligence questions attempted within time limit
f21003 2 0	age when attended assessment centre
2 0	total hours walked 10 minutes
2 0	total hours moderate physical activity 10 minutes
2 0	total hours vigorous physical activity 10 minutes
2 0	total hours of walking for pleasure in last 4 weeks
2 0	total hours of strenuous sports in last 4 weeks
2 0	total hours of other exercises in last 4 weeks
2 0	total hours of light diy in last 4 weeks
2 0	total hours of heavy diy in last 4 weeks
2 0	number of physical activities wrt walking for pleasure
2 0	years since first sexual intercourse
2 0	years since started wearing glasses
2 0	log time to answer
2 0	inverse log duration screen displayed
2 0	inverse log number of attempts
2 0	log pm score
2 0	fluid intelligence interaction
f31 0 0	sex

The 26 variables are common to all of the modality-specific MANCOVA models. The interaction between age and sex is also included for each of the modality-specific MANCOVA models. In addition to the 27 common variables, sMRI and dMRI modalities have 1 nuisance variable (rspatialNorm: correlation between individual GM/FA map to the site-specific mean) and fMRI has 2 nuisance

variables (rspatialNorm, and meanFD: estimated mean framewise displacement of the subject during the scan).

For brain-age delta analysis, we use a different subset of 42 variables from the original 64 variables. Those variables are listed in Figures 5, S3, S4, and S5.

S1.3. Preprocessing Details

UK Biobank: **sMRI** The images underwent segmentation and normalization to MNI space using the SPM12 toolbox, yielding GM, white matter (WM), and cerebro-spinal fluid (CSF) tissue probability maps. The normalized GM segmentations were spatially smoothed using a 10mm FWHM Gaussian filter. The smoothed images were resampled to $3\times3\times3\text{mm}^3$. We defined a group mask to restrict the analysis to GM voxels as follows. First, an average GM segmentation map from all subjects was obtained from the normalized GM segmentation maps at 1mm^3 resolution. This map was binarized at a 0.2 threshold (classify voxels with a group average probability > 0.2 as gray matter) and resampled to $3\times3\times3\text{mm}^3$ resolution, which resulted in $V_m = 44{,}318$ in-brain voxels. **rs-fMRI** We used distortion corrected, FIX-denoised (Griffanti et al., 2014), normalized rs-fMRI data provided by the UK Biobank data resource to compute subject-specific ALFF maps, defined as the area under the low frequency band [0.01-0.08 Hz] power spectrum of each voxel time course in a given scan. We then obtained mean-scaled ALFF maps (mALFF), which are subject-specific ALFF maps divided by their global mean ALFF value, since this scaling has been shown to result in greater test-retest reliability of ALFF maps (Zhao et al., 2018). The mALFF maps were smoothed using a 6mm FWHM Gaussian filter and resampled to $3\times3\times3\text{mm}^3$ isotropic voxels. We used the same group mask learned from GM features for mALFF maps in the subsequent fusion analysis. **dMRI** The FA maps provided by the UK Biobank consortium were used. The preprocessing steps that raw dMRI images underwent are thoroughly described in (Alfaro-Almagro et al., 2018). The FA maps were then spatially smoothed using a 6mm FWHM Gaussian filter and resampled to $3\times3\times3\text{mm}^3$ voxels. For dMRI data, we computed a group mask similar to the approach described above for sMRI data. However, the group average WM segmentation was binarized at a threshold of 0.4, resulting in $V_m = 18{,}684$ in-brain voxels in the group mask.

Patient Datasets: **sMRI** All datasets underwent the same preprocessing steps (Qi et al., 2022): data were normalized to MNI space using the unified segmentation method in SPM12, resliced to 3mm^3, and segmented into gray matter (GM), white matter (WM), and cerebral spinal fluid (CSF) using modulated normalization, yielding results such as gray matter volume (GMV). The GMV maps were then smoothed using a Gaussian kernel with a full width at half maximum (FWHM)

= 6 mm. Subject outlier detection was further performed using a spatial Pearson correlation with the template image to ensure that all subjects were properly segmented. **rs-fMRI** All datasets underwent the same preprocessing (Qi et al., 2022) based on statistical parametric mapping (SPM12, http://www.fil.ion.ucl.ac.uk/spm/) under a MATLAB 2019 environment. It included the following steps: 1) the first five scans were discarded to remove T1 equilibration effects 2) slice timing correction; 3) realignment; 4) normalization to the EPI template with $3\times3\times3mm^3$ resolution; 5) spatial smoothing using a 6mm FWHM Gaussian kernel. After that, 6) nuisance covariates (6 head motions + CSF + WM) + global signal were regressed out via a general linear model from the voxel time series, and 7) calculation of mALFF. **dMRI** *COBRE and BSNIP*: The dMRI data were processed with the following steps (Caprihan et al., 2011). Motion and eddy current correction: Given a 4D DTI volume and a table of corresponding b-values and gradient direction vectors, we registered all the images to a b=0 s/mm^3 image, and a 12 degrees of freedom affine transformation with mutual information cost function was used for image registration. Adjusting the diffusion gradient direction: Two corrections were applied to the diffusion gradients. The nominal diffusion gradient directions were prescribed in the magnet axis frame. We rotated them to correspond to the image slice orientation. No correction was required if the imaging slice was pure axial. A second correction accounted for any image rotation during the previous motion and eddy current correction step. The rotation part of the transformation previously found was extracted, and each gradient direction vector was accordingly corrected. All the image registration and transformations were done with FLIRT. Dtifit, a tool in FSL, was adopted to calculate the diffusion tensor and the FA maps. The FA image was aligned to an Montreal Neurologic Insititute (MNI) FA template with FNIRT and resliced via SPM, resulting in a final voxel size of $2\times2\times2$ mm^3. *fBIRN*: DMRI data were preprocessed with the following steps (Qi et al., 2018b): 1) quality check with any gradient directions with excessive motion or vibration artifacts identified and removed; 2) motion and eddy current correction; 3) correction of gradient directions for any image rotation done during the previous motion correction step; and 4) calculation of diffusion tensor. *MPRC*: FA images were created by fitting the diffusion tensor voxel-wise, after correcting the data for head motion and eddy-current distortion (Wright et al., 2015). Average head motion during the scans was measured during spatial alignment of diffusion-sensitized images to the b = 0 image. The RMSDIFF program, distributed with FSL was used to estimate the root mean square (RMS) movement distance between diffusion sensitized and b = 0 images. All data passed a quality assurance control of less than 3 mm accumulated motion during the scan. Then, all FA images were globally spatially normalized to the Johns Hopkins University (JHU) atlas that is distributed with the FSL package.

The patient datasets were Gaussian smoothed, with filter FWHM = 10mm (GM), 6mm (mALFF), 6mm (FA), and resampled to $3\times3\times3mm^3$ resolution. The same masks defined for UK Biobank were used in the patient datasets.

S1.4. Aging Effects

Five SCVs (3, 5, 8, 16, 17) were significantly associated with age identified by the MANCOVA analysis.

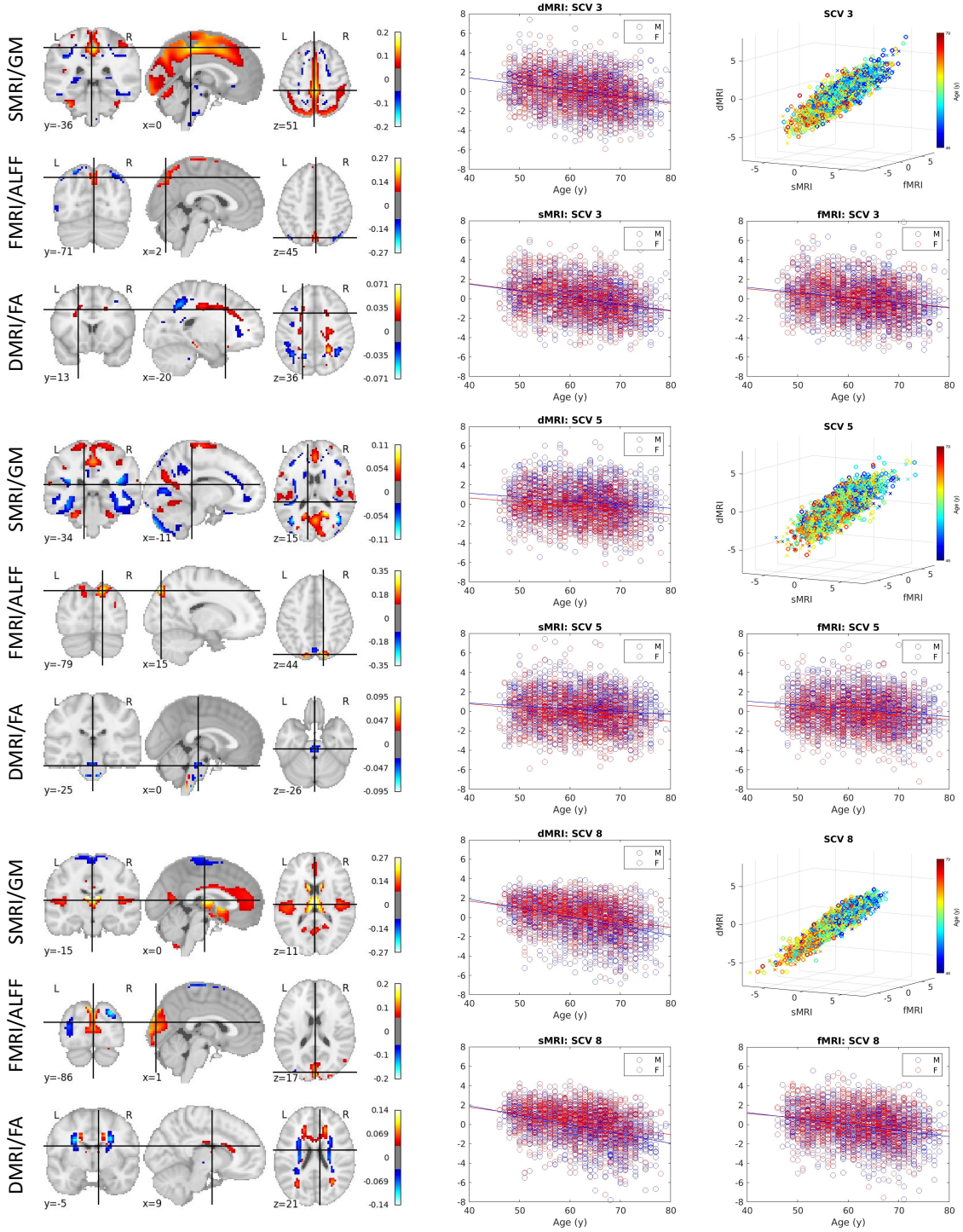

(a) SCVs 3, 5, and 8

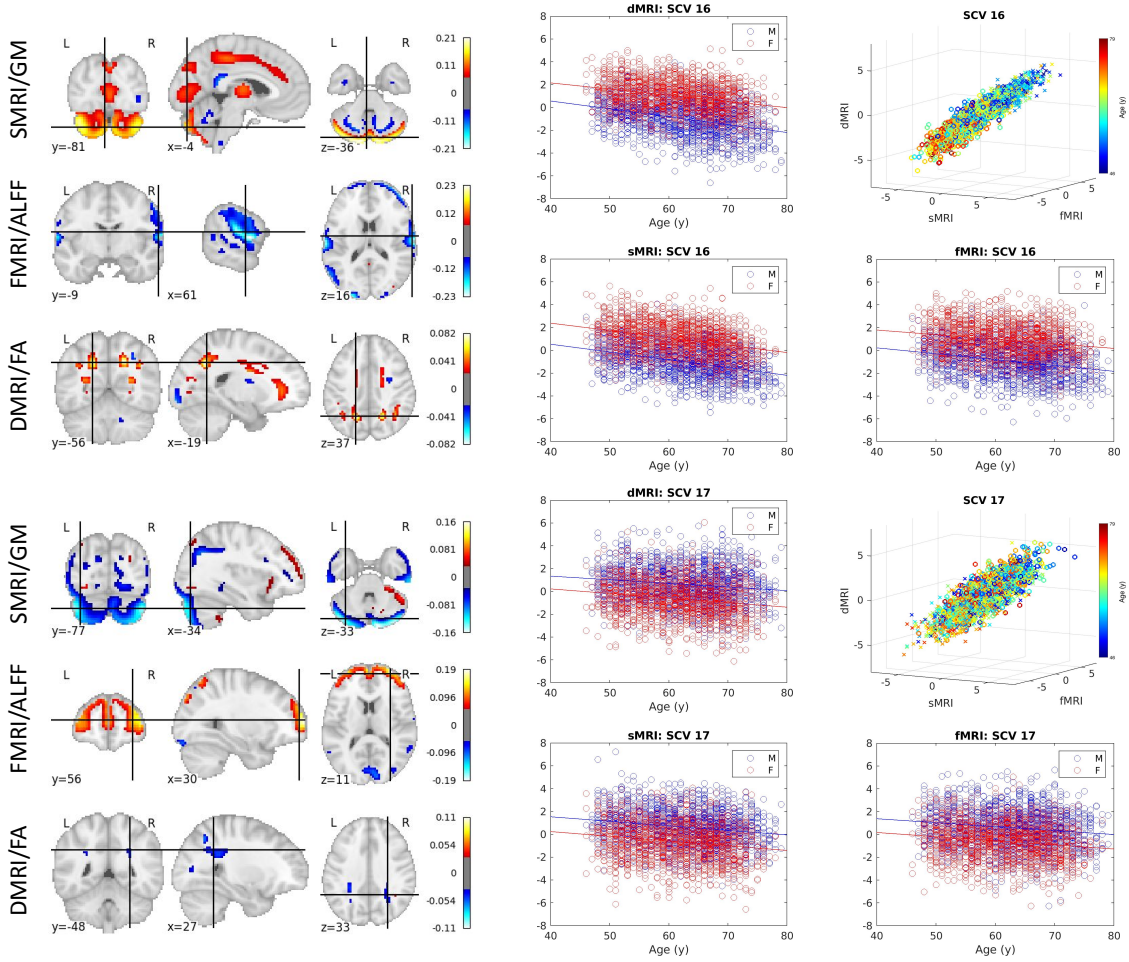

(b) SCVs 16 and 17

Figure S1: **Age-related SCV**. Right: 3D scatter plots of SCVs 3, 5, 8, 16, 17 illustrate the association between the identified multimodal subject expression levels and age for UK Biobank data. Each point represents a subject, color coded by the age (circles indicate females; crosses indicate males). Left: The spatial maps corresponding to the mixing weights for each modality are also shown.

S1.5. Brain-age Delta Modeling

S1.5.1. Estimation Details

In the first step of brain-age delta modeling, the subject expression levels (the top SVD-shared feature plus the partialled sMRI and fMRI features) from five SCVs with significant age effect size (based on the multivariate MANCOVA assessment in Section 2.6) were used to predict age. Thus, the initial estimate of brain-age delta was evaluated as:

$$\delta_1 = X\boldsymbol{\beta}_1 - Y, \tag{11}$$

where Y is the actual age after removing the mean age across subjects, X is the matrix of significant age-related SCVs with size $N \times \bar{C}$ (N = number of subjects, $\bar{C} = 5$ SVD-shared features + 5 sMRI sources + 5 dMRI sources = 15), and $\boldsymbol{\beta}_1$ is the $\bar{C} \times 1$ vector of regression parameters. As such, δ_1 shows the aging effects that cannot be captured by the imaging modalities, with positive values suggesting accelerated aging and negative values suggesting slowed down aging.

In the second step of brain-age delta modeling, the model is refined to identify aspects of δ_1 that cannot be captured by age terms (notice that δ_1 is by definition dependent on age) nor confounds, such as sex. Thus, δ_2 is evaluated as:

$$\delta_2 = \delta_1 - Y_2\boldsymbol{\beta}_2, \tag{12}$$

where the regression matrix Y_2 includes the demeaned linear age term, the demeaned quadratic age term after regressing out the linear age effects and normalizing to have the same standard deviation as the linear age term, the demeaned cubic age term after regressing out the linear and quadratic age effects and normalizing to have the same standard deviation as the linear age term, sex, the interaction between sex and each of the three age terms, the framewise displacement variable, and the spatial normalization variables from the three modalities. Note that after each effect removal step, the mean of the adjusted variable was removed again. $\boldsymbol{\beta}$ regression coefficients are estimated as usual by $\boldsymbol{\beta}_1 = (X^\top X)^{-1}X^\top Y$ and $\boldsymbol{\beta}_2 = (Y_2^\top Y_2)^{-1}Y_2^\top \delta_1$.

Following that, source-specific contributions to the overall brain age delta can be determined, yielding source-specific delta vectors, δ_{1i} and δ_{2i}, as follows. First, note that the source-specific contributions can be combined to recover the original Y (here, $\frac{1}{\bar{C}}$ is arbitrary and irrelevant since age effects are removed in the following step, thus we set $\frac{1}{\bar{C}} = 0$):

$$X\boldsymbol{\beta}_1 - \delta_1 = \sum_{i=1}^{\bar{C}}(X_i\beta_{1i} - \delta_{1i}) = \sum_{i=1}^{\bar{C}}\frac{1}{\bar{C}}Y = Y. \tag{13}$$

The source-specific delta vector at the first stage, δ_{1i}, can be calculated by:

$$\delta_{1i} = X_i \beta_{1i} - \frac{Y}{\bar{C}}. \tag{14}$$

In the next step, we compute the regression coefficients $\boldsymbol{\beta}_{2i} = (Y_2^\top Y_2)^{-1} Y_2^\top \delta_{1i}$, and the source-specific delta vector at the second stage is obtained:

$$\delta_{2i} = \delta_{1i} - Y_2 \boldsymbol{\beta}_{2i}. \tag{15}$$

We removed the mean of the δ_{2i} at the end. We repeated the above source-specific brain-age delta estimation process (14) and (15) for each source in each age-related SCV.

We then computed the final source-specific 2-stage brain-age *partialled* δ_{2i} by regressing out other δ_{2i} vectors from each particular δ_{2i} vector.

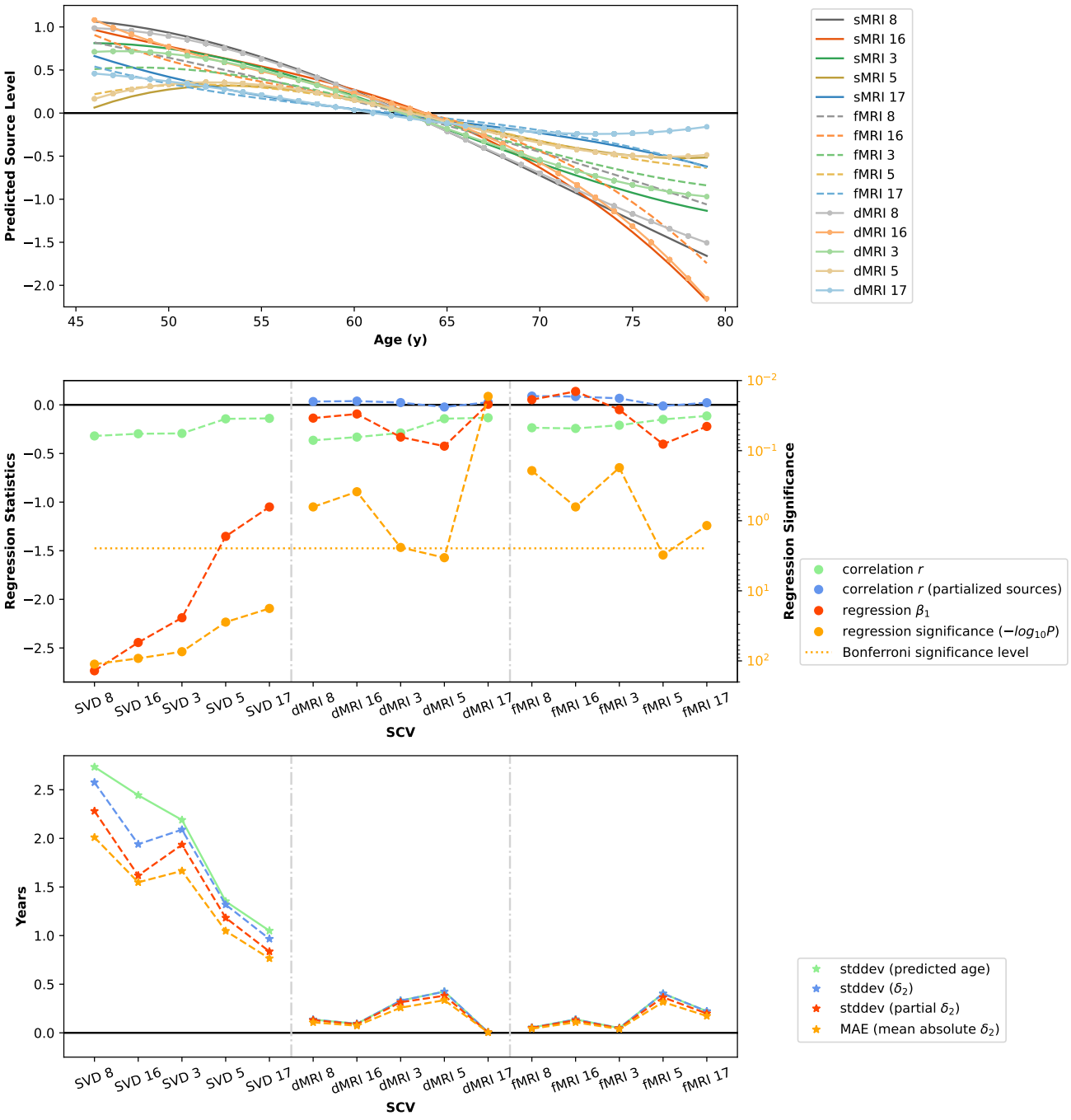

Figure S2: **Brain age delta modeling (dMRI)**. Top: Predicted source levels as a function of brain age using a cubic model. Middle: Regression statistics at stage 1 of brain-age delta modeling ($age = S * \boldsymbol{\beta}_1$). Bottom: Standard deviation of predicted age, standard deviation of estimated stage 2 brain-age delta, and mean absolute error in stage 2 brain-age model. SCVs are sorted according to the correlation between the age and the source within each modality.

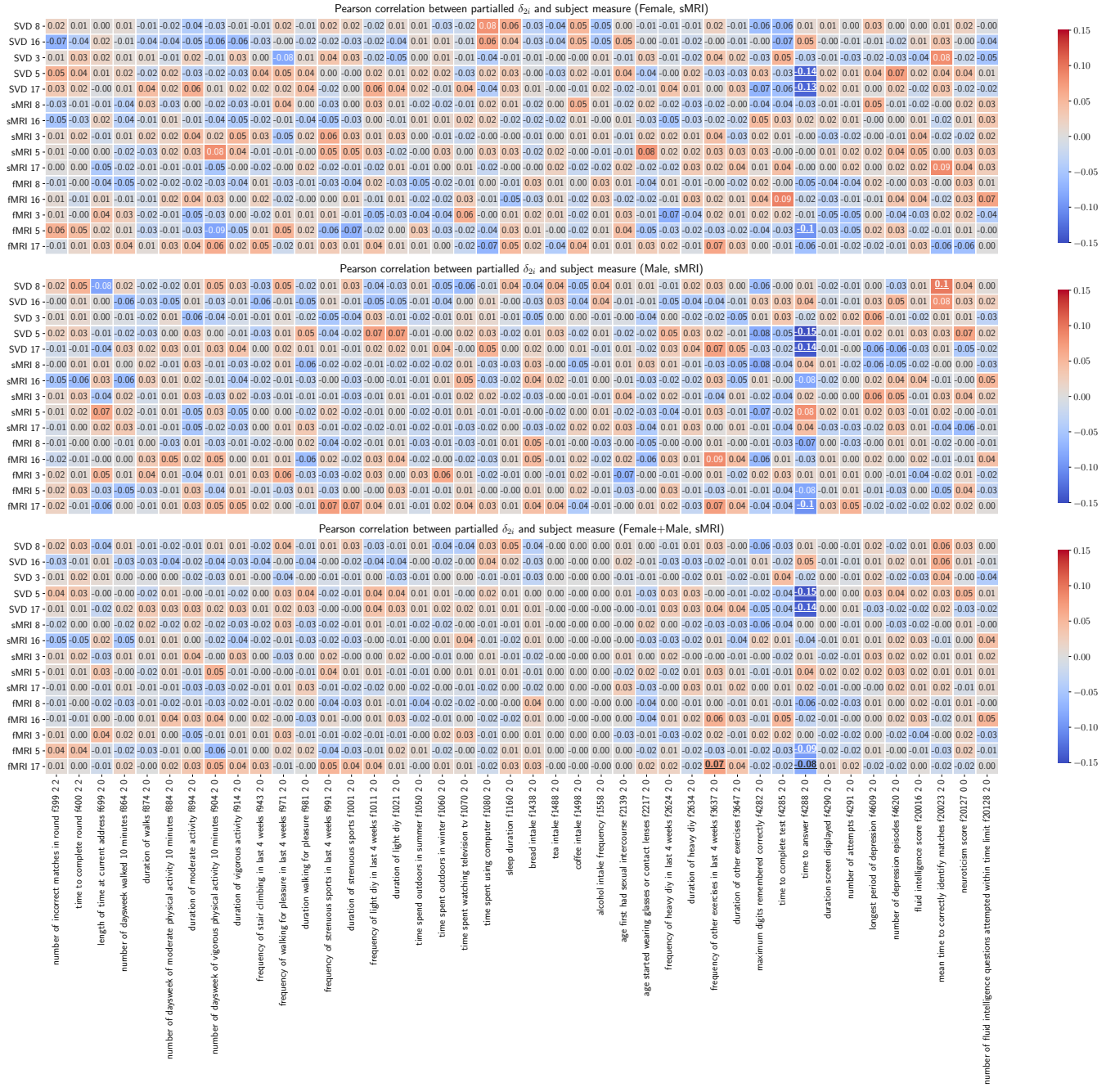

Figure S3: **Pearson correlations between partialled δ_{2i} vectors (sMRI) and subject measures**. Pearson correlations are calculated between 15 partialled δ_{2i} vectors and 42 variables for each gender and for all subjects. The underscored correlations are significant.

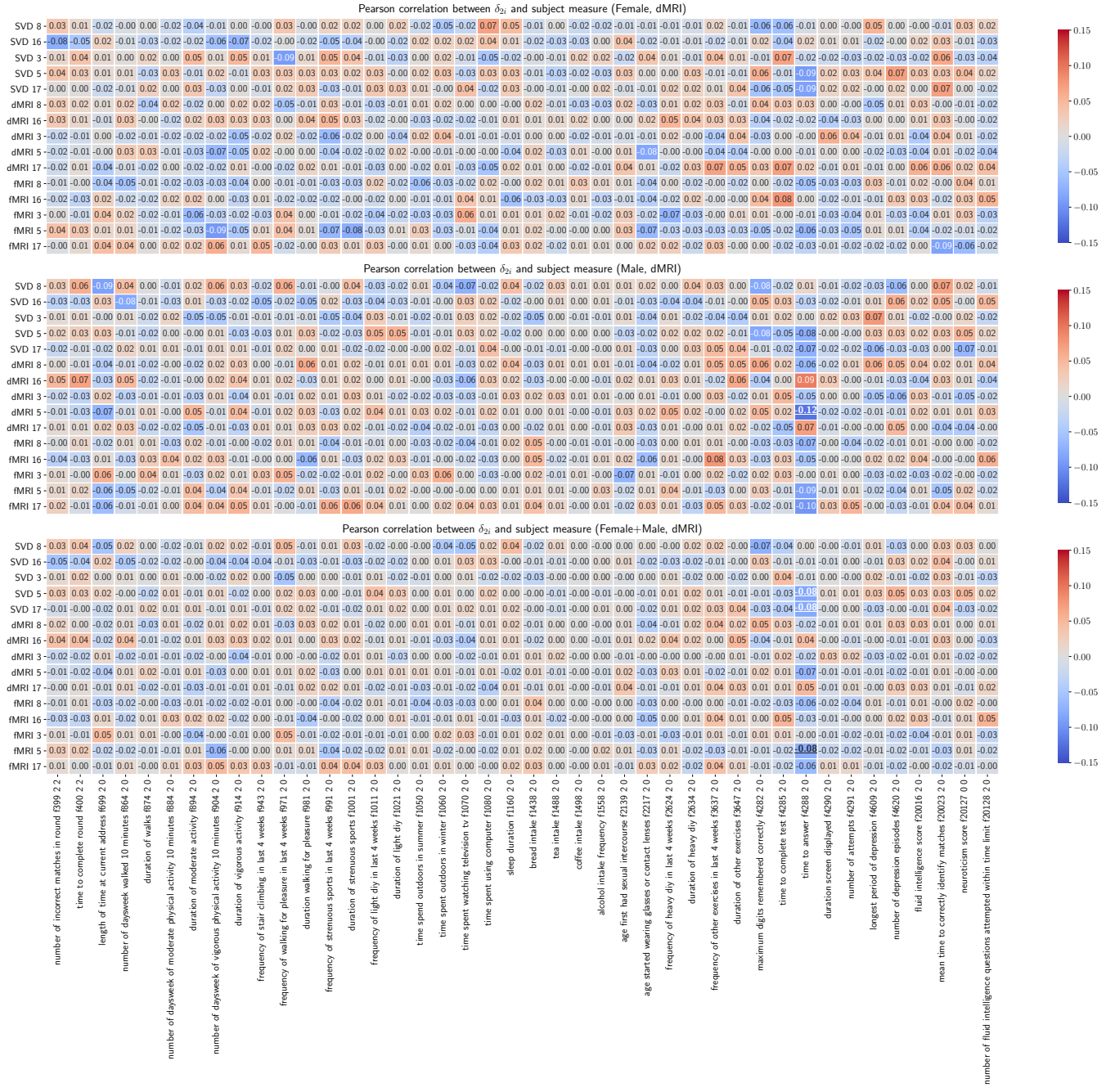

Figure S4: **Pearson correlations between δ_{2i} vectors (dMRI) and subject measures**. Pearson correlations are calculated between 15 δ_{2i} vectors and 42 variables for each gender and for all subjects. The underscored correlations are significant.

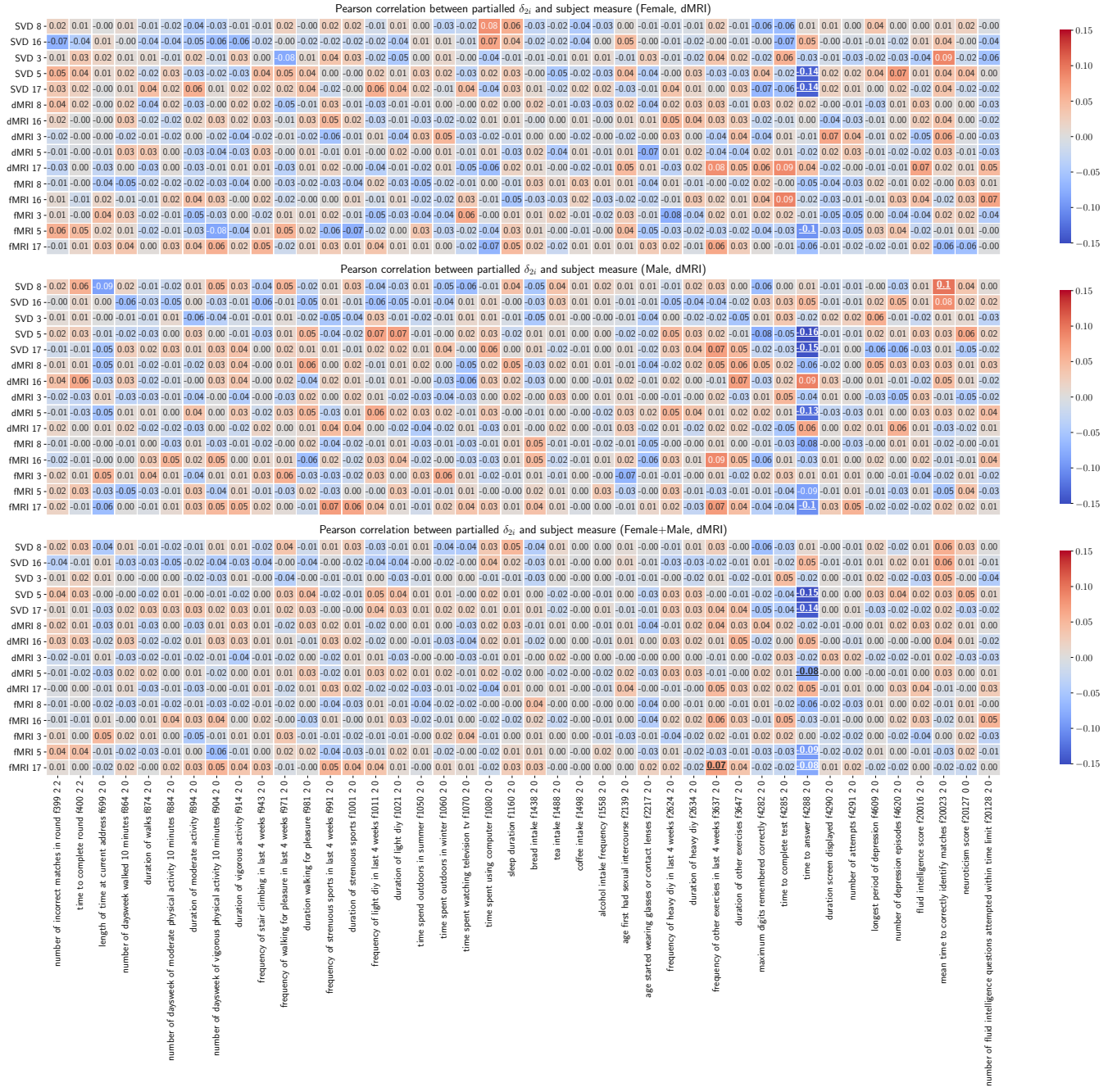

Figure S5: **Pearson correlations between partialled δ_{2i} vectors (dMRI) and subject measures**. Pearson correlations are calculated between 15 partialled δ_{2i} vectors and 42 variables for each gender and for all subjects. The underscored correlations are significant.

S1.6. Sex Effects

SCVs (9, 10, 17, 22) were significantly associated with sex identified by the MANCOVA analysis and the effect size measure.

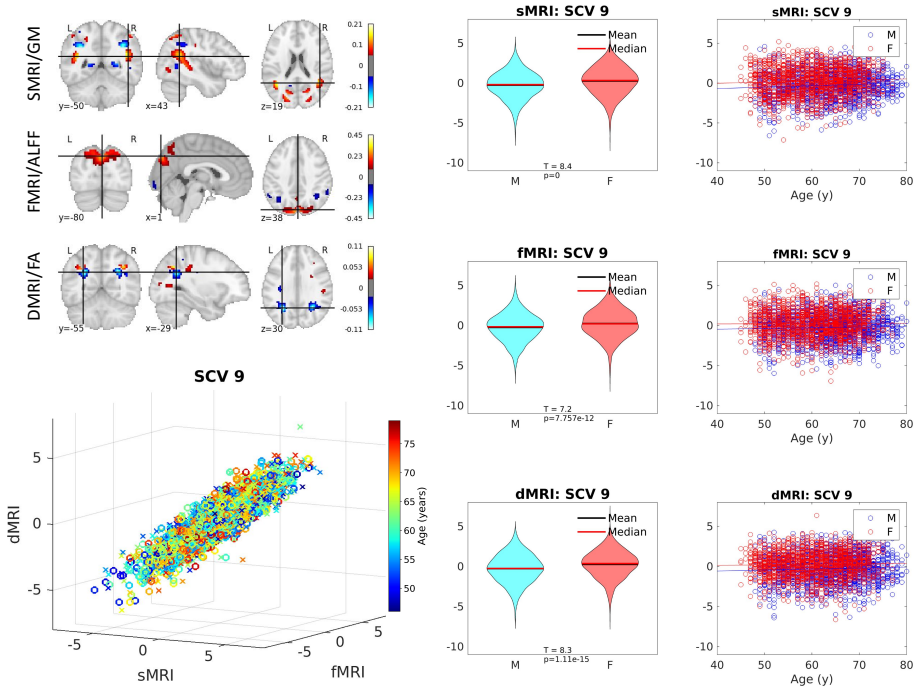

(a) SCV 9

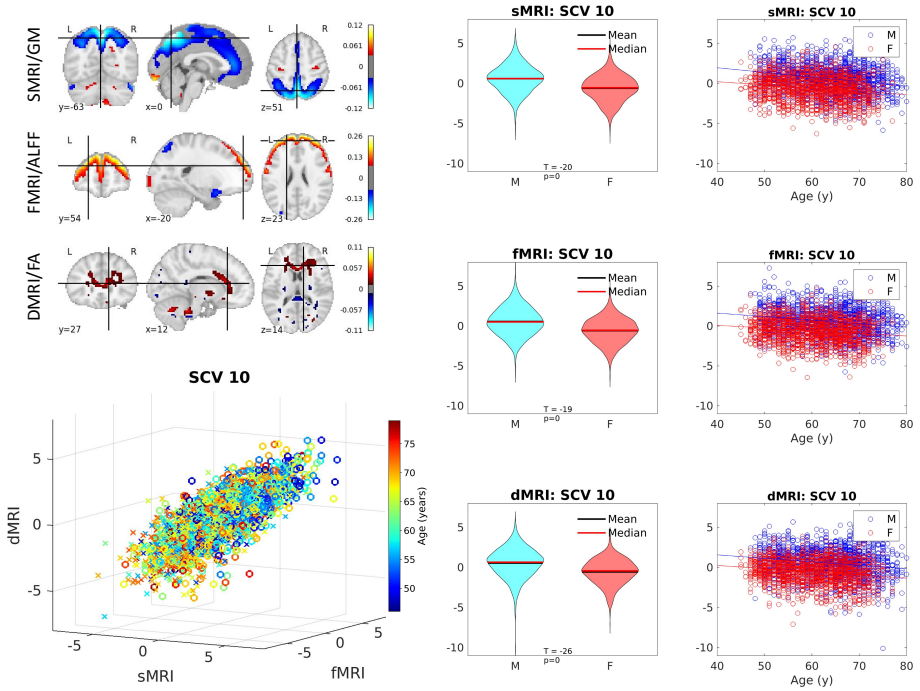

(b) SCV 10

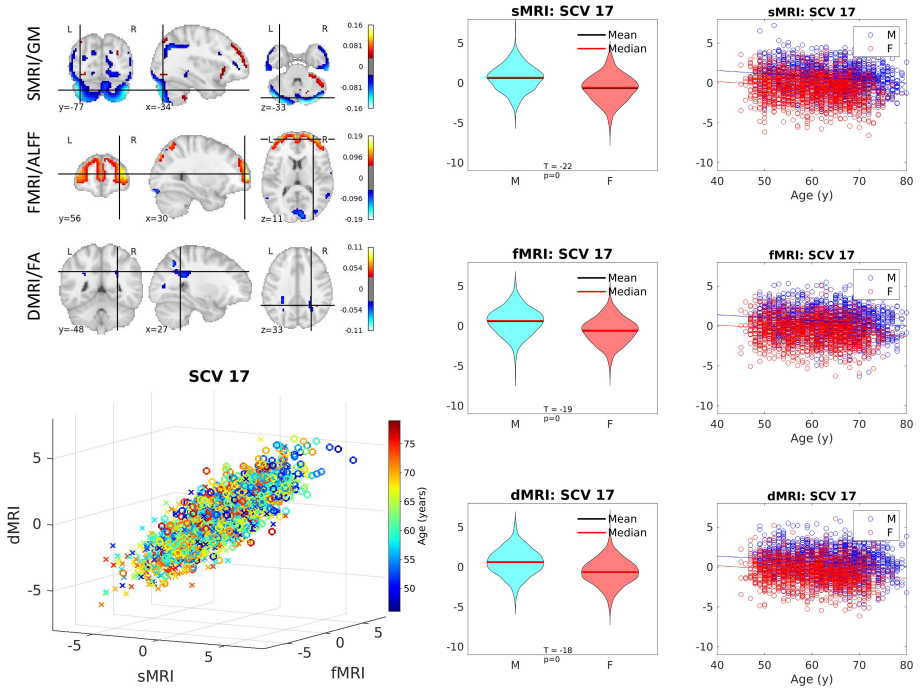

(c) SCV 17

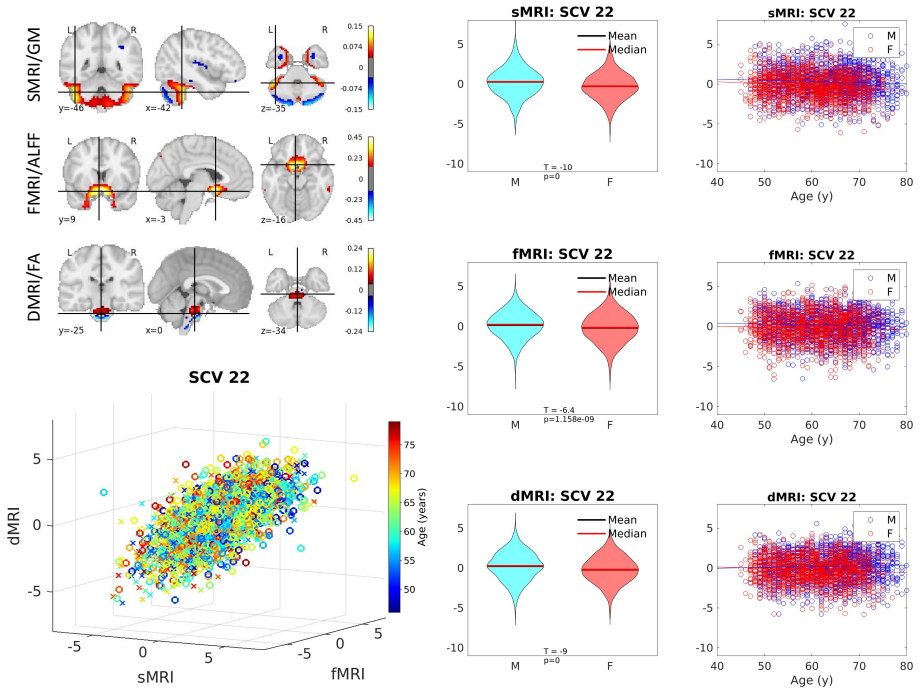

(d) SCV 22

Figure S6: **Sex-related SCV**. Illustration of SCVs 9, 10, 17 and 22. **In each SCV sub-panel**: Top left: Spatial maps. Bottom left: Multimodal subject expression level sources, depicting all subjects (colored by age). Right: Source intensity differences related to sex effects.

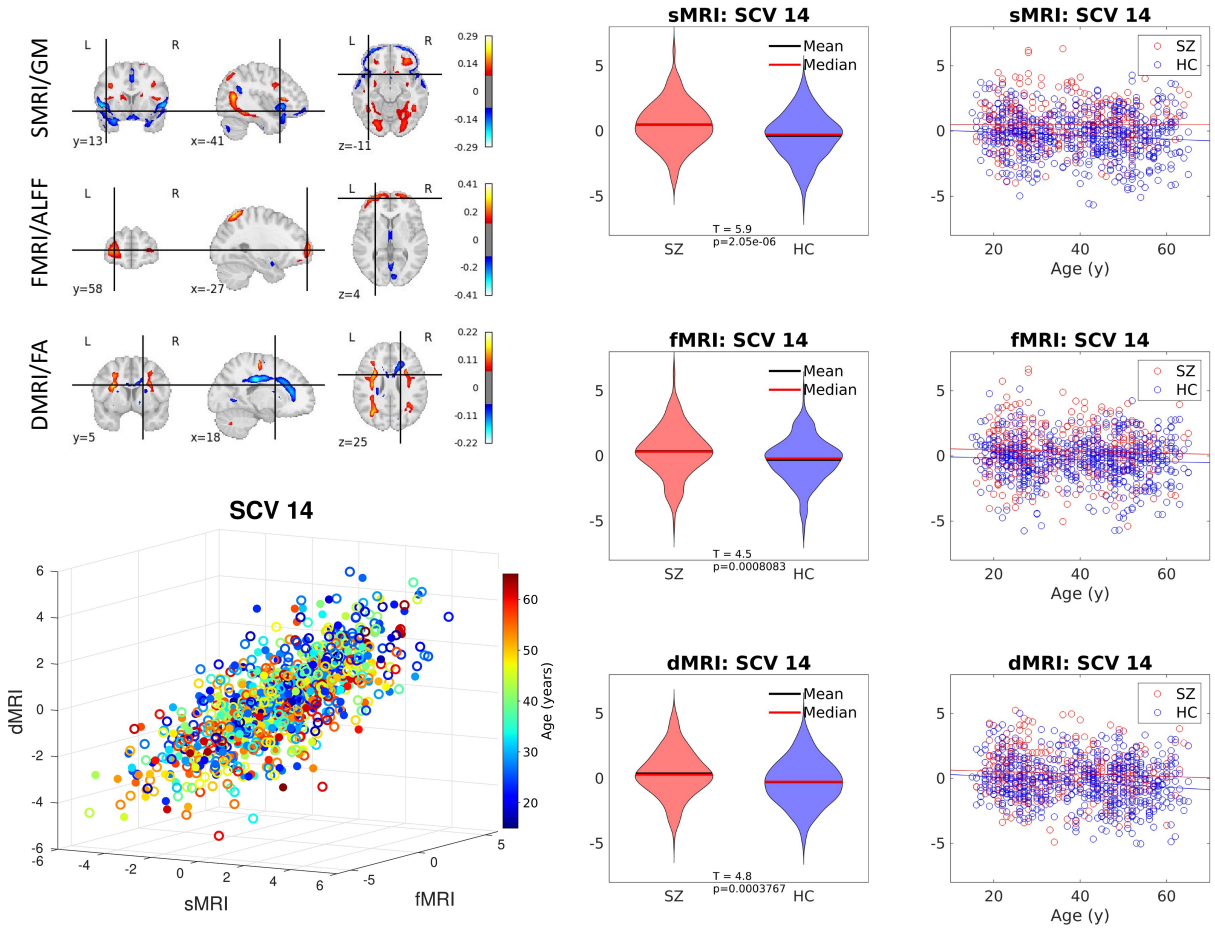

Figure S7: **Schizophrenia-related SCV**. Illustration of SCV 14. Top left: Spatial maps. Bottom left: Multimodal subject expression level sources, depicting all subjects (colored by age). Right: Source intensity differences related to schizophrenia effects.

S1.8. Effect Size Measure (UK Biobank Dataset)

We fit a linear regression model using phenotype scores to predict SCVs for each of three modalities. Specific phenotypes showing significant association from MANCOVA for each modality are listed as follows:

- sMRI: sex, time spent watching television, age first had sexual intercourse, time to answer, fluid intelligence score, age when attended assessment centre, first principal component of physical exercise variables, spatial normalization, sex and age interaction.
- fMRI: alcohol intake frequency, sex, sleep duration, age first had sexual intercourse, time to answer, fluid intelligence score, age when attended assessment centre, third principal component of physical exercise variables, spatial normalization, mean framewise displacement, sex and age interaction.
- dMRI: sex, time spent watching television, time to answer, fluid intelligence score, mean time to correctly identify matches, age when attended assessment centre, spatial normalization, sex and age interaction.

For a categorical variable with more than two categories, such as alcohol intake frequency with six categories, we fit another linear regression model without the categorical variable, namely a reduced model. We obtained the statistics of the categorical variable from the ANOVA analysis between the reduced model and full model.

We replaced Type II effect size measures with Type III effect size measures for SCVs having significant age and sex interactions. The SCVs below have significant age and sex interactions ($p < 0.05$, Bonferroni correction) and their Type II effect size measures are replaced by Type III effect size measures:

- sMRI: 6, 11, 18, 21, 23, 24, 28.
- fMRI: 18, 25.
- dMRI: 6, 18, 22, 26.

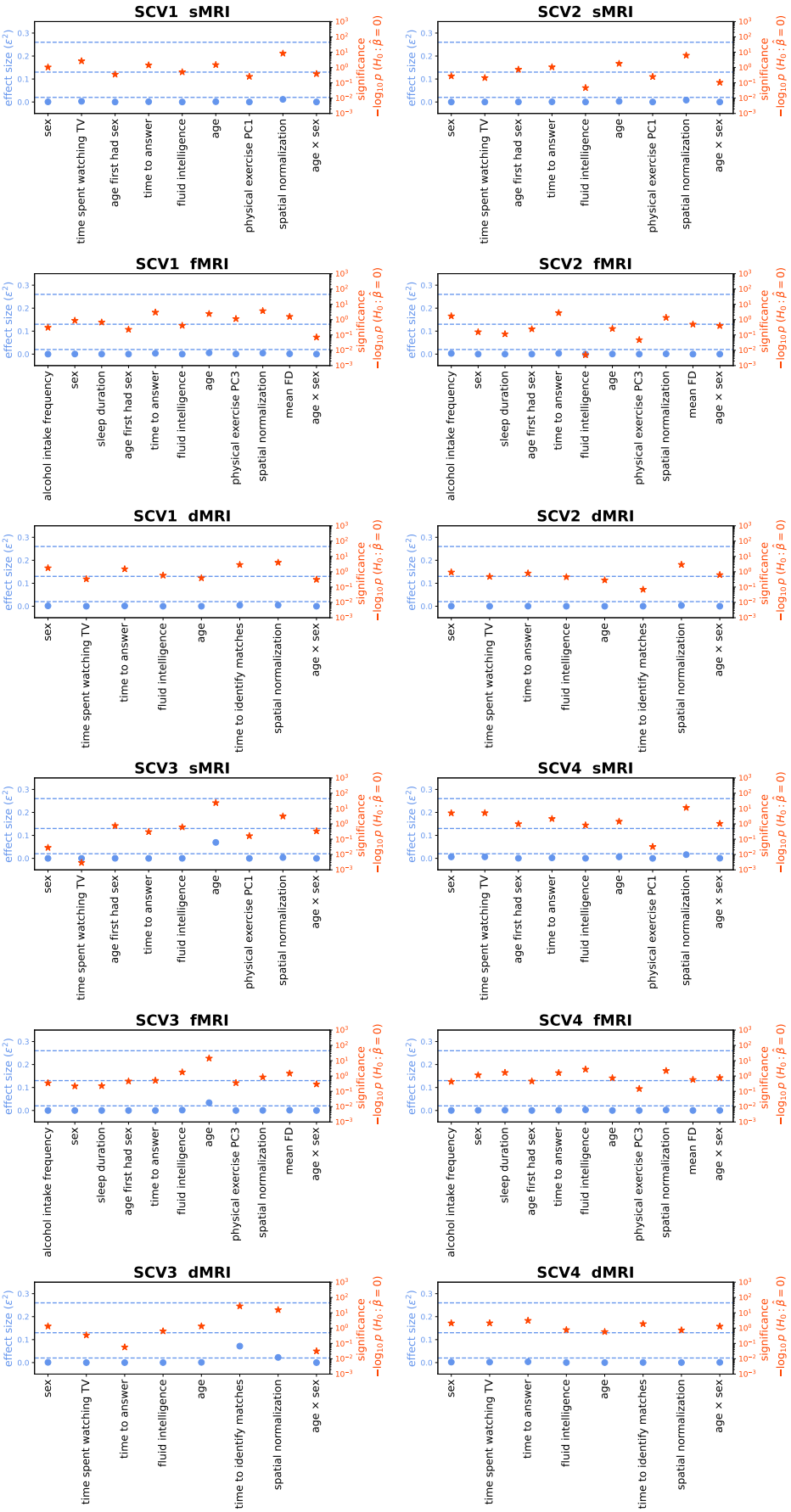
SCV1 sMRI
SCV2 sMRI
SCV1 fMRI
SCV2 fMRI
SCV1 dMRI
SCV2 dMRI
SCV3 sMRI
SCV4 sMRI
SCV3 fMRI
SCV4 fMRI
SCV3 dMRI
SCV4 dMRI
effect size (ε^2)
significance
$-\log_{10} p\ (H_0 : \hat{\beta} = 0)$
sex
time spent watching TV
age first had sex
time to answer
fluid intelligence
age
physical exercise PC1
spatial normalization
age × sex
alcohol intake frequency
sleep duration
physical exercise PC3
mean FD
time to identify matches

(a) SCVs 1-4

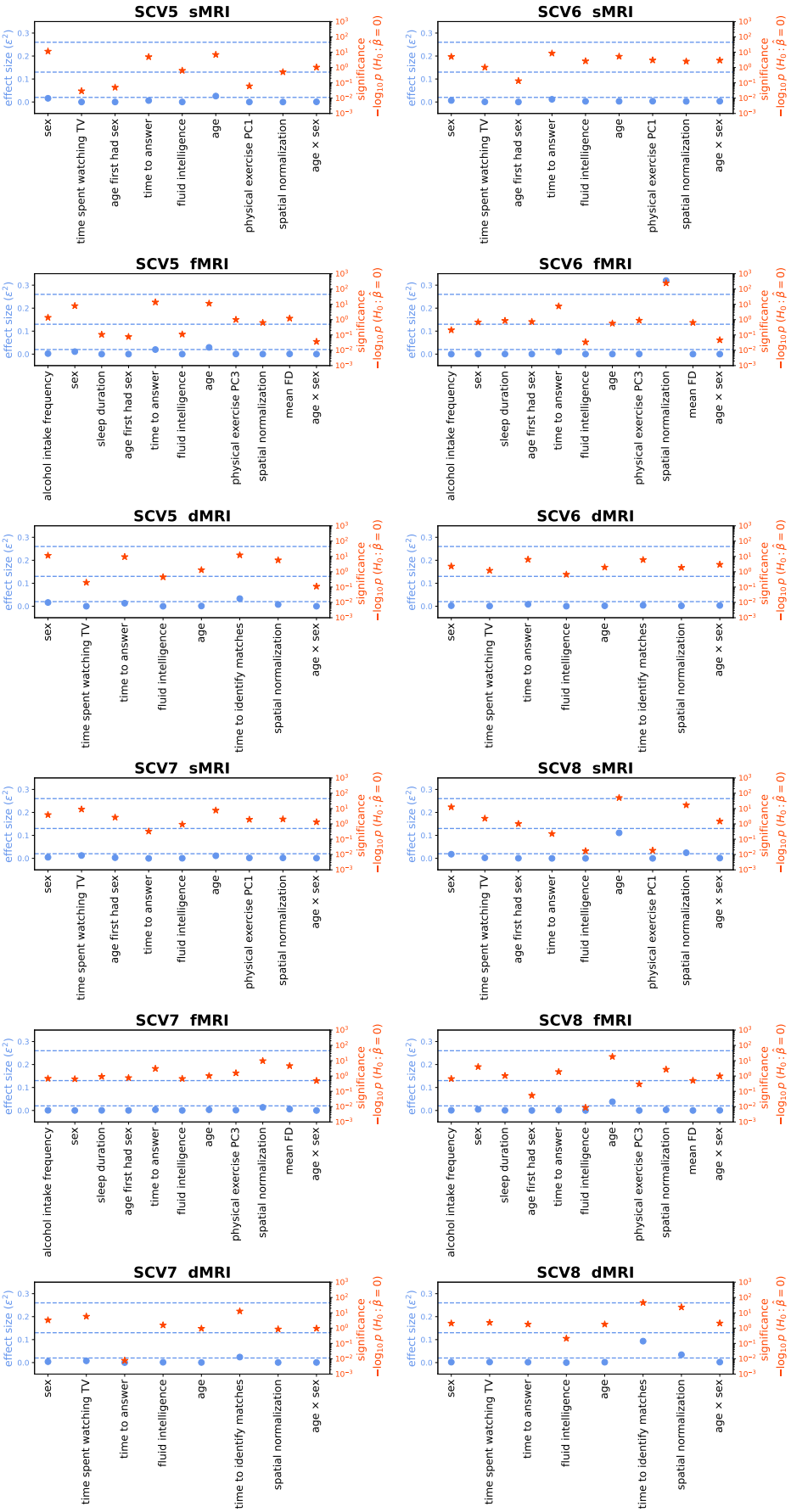
SCV5 sMRI
SCV6 sMRI
SCV5 fMRI
SCV6 fMRI
SCV5 dMRI
SCV6 dMRI
SCV7 sMRI
SCV8 sMRI
SCV7 fMRI
SCV8 fMRI
SCV7 dMRI
SCV8 dMRI
effect size (ε^2)
significance
$-\log_{10} p\ (H_0 : \hat{\beta} = 0)$
sex
time spent watching TV
age first had sex
time to answer
fluid intelligence
age
physical exercise PC1
spatial normalization
age × sex
alcohol intake frequency
sleep duration
physical exercise PC3
mean FD
time to identify matches

(b) SCVs 5-8

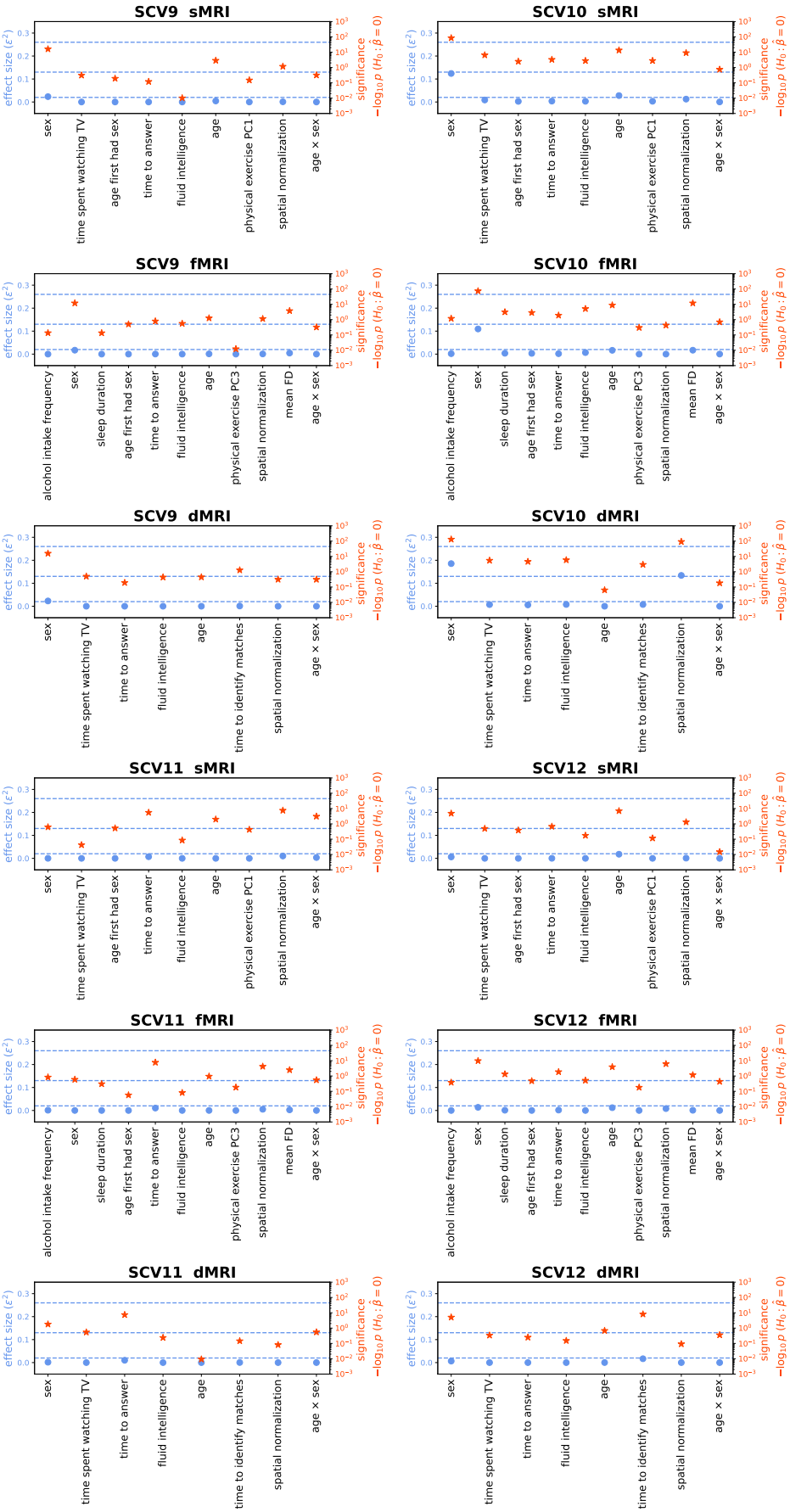
SCV9 sMRI
SCV10 sMRI
SCV9 fMRI
SCV10 fMRI
SCV9 dMRI
SCV10 dMRI
SCV11 sMRI
SCV12 sMRI
SCV11 fMRI
SCV12 fMRI
SCV11 dMRI
SCV12 dMRI
effect size (ε^2)
significance
$-\log_{10} p\ (H_0 : \hat{\beta} = 0)$
sex
time spent watching TV
age first had sex
time to answer
fluid intelligence
age
physical exercise PC1
spatial normalization
age × sex
alcohol intake frequency
sleep duration
physical exercise PC3
mean FD
time to identify matches

(c) SCVs 9-12

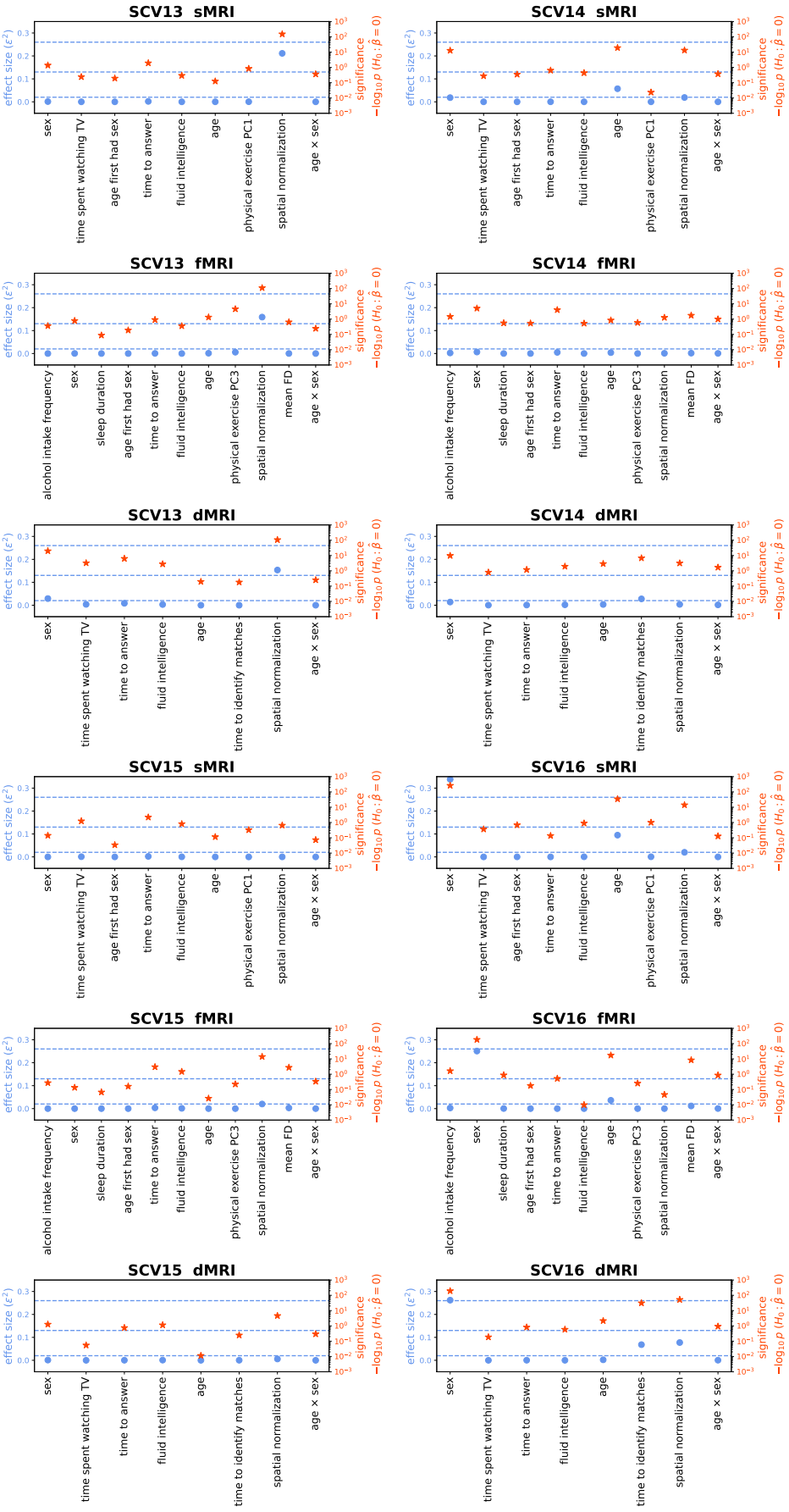
SCV13 sMRI
SCV14 sMRI
SCV13 fMRI
SCV14 fMRI
SCV13 dMRI
SCV14 dMRI
SCV15 sMRI
SCV16 sMRI
SCV15 fMRI
SCV16 fMRI
SCV15 dMRI
SCV16 dMRI
effect size (ε^2)
significance
$-\log_{10} p\ (H_0 : \hat{\beta} = 0)$
sex
time spent watching TV
age first had sex
time to answer
fluid intelligence
age
physical exercise PC1
spatial normalization
age × sex
alcohol intake frequency
sleep duration
physical exercise PC3
mean FD
time to identify matches

(d) SCVs 13-16

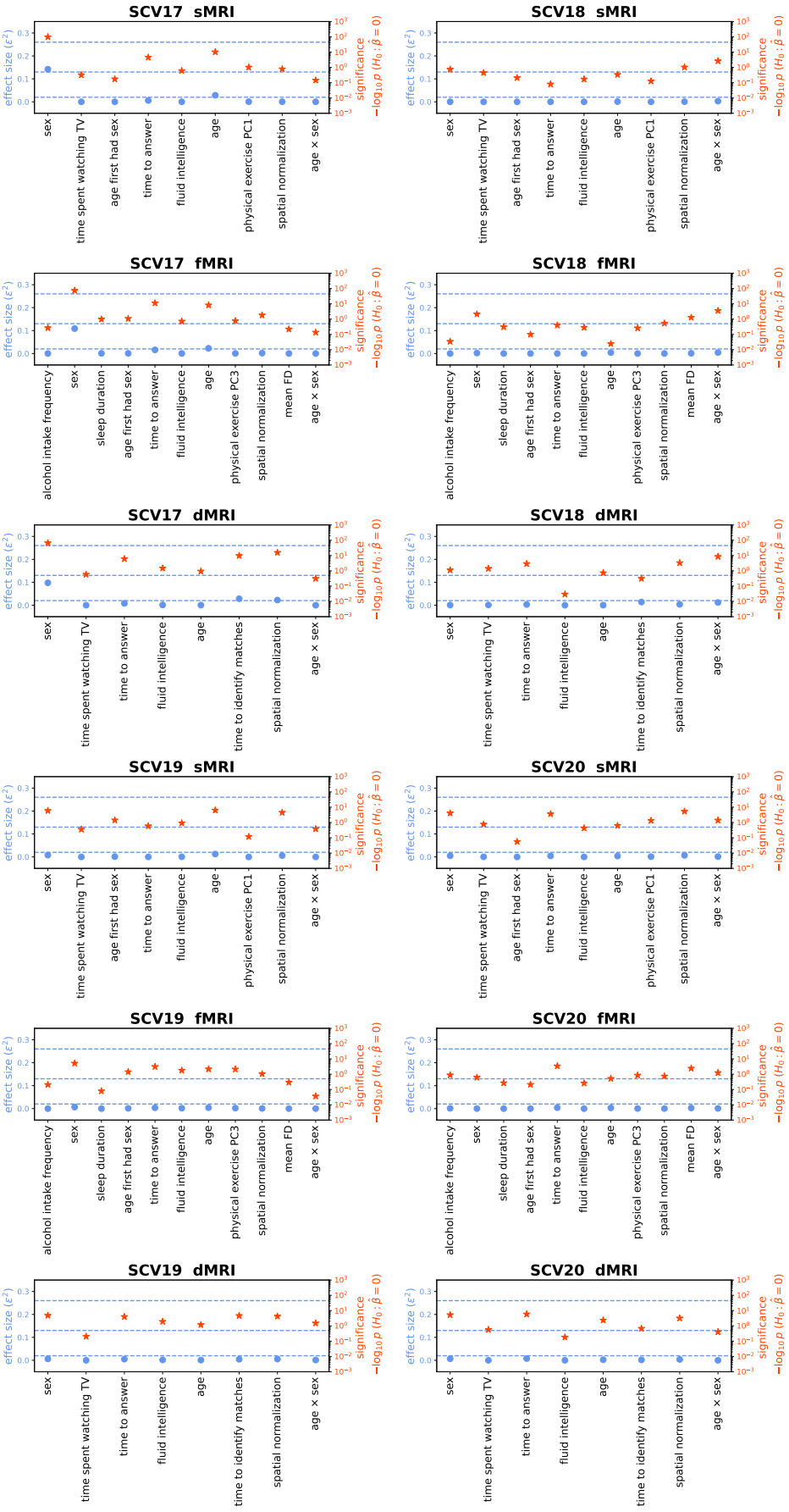
SCV17 sMRI
SCV18 sMRI
SCV17 fMRI
SCV18 fMRI
SCV17 dMRI
SCV18 dMRI
SCV19 sMRI
SCV20 sMRI
SCV19 fMRI
SCV20 fMRI
SCV19 dMRI
SCV20 dMRI
effect size (ε^2)
significance
$-\log_{10} p\ (H_0 : \hat{\beta} = 0)$
sex
time spent watching TV
age first had sex
time to answer
fluid intelligence
age
physical exercise PC1
spatial normalization
age × sex
alcohol intake frequency
sleep duration
physical exercise PC3
mean FD
time to identify matches

(e) SCVs 17-20

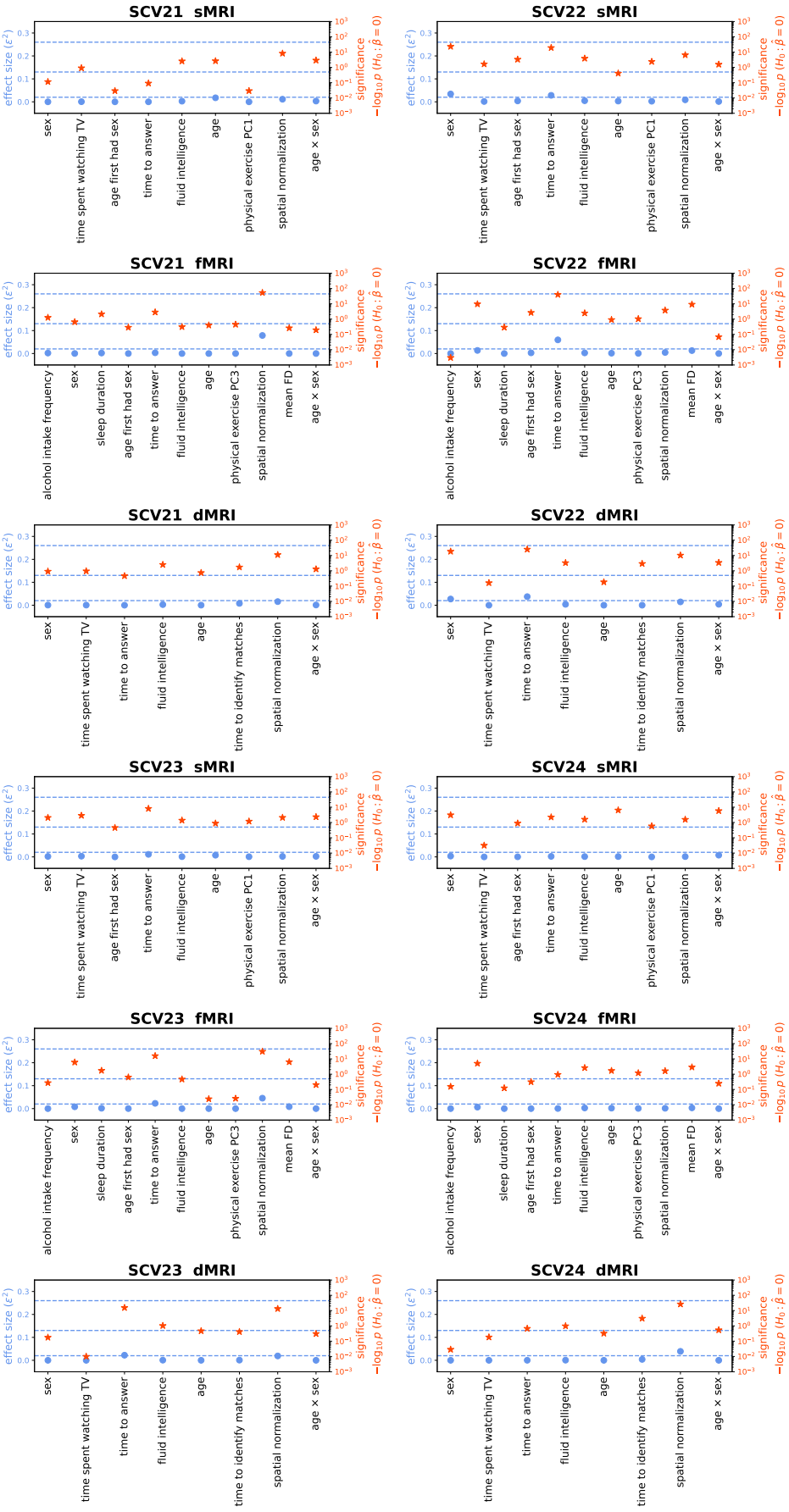
SCV21 sMRI
SCV22 sMRI
SCV21 fMRI
SCV22 fMRI
SCV21 dMRI
SCV22 dMRI
SCV23 sMRI
SCV24 sMRI
SCV23 fMRI
SCV24 fMRI
SCV23 dMRI
SCV24 dMRI
effect size (ε^2)
significance
$-\log_{10} p\ (H_0 : \hat{\beta} = 0)$
sex
time spent watching TV
age first had sex
time to answer
fluid intelligence
age
physical exercise PC1
spatial normalization
age × sex
alcohol intake frequency
sleep duration
physical exercise PC3
mean FD
time to identify matches

(f) SCVs 21-24

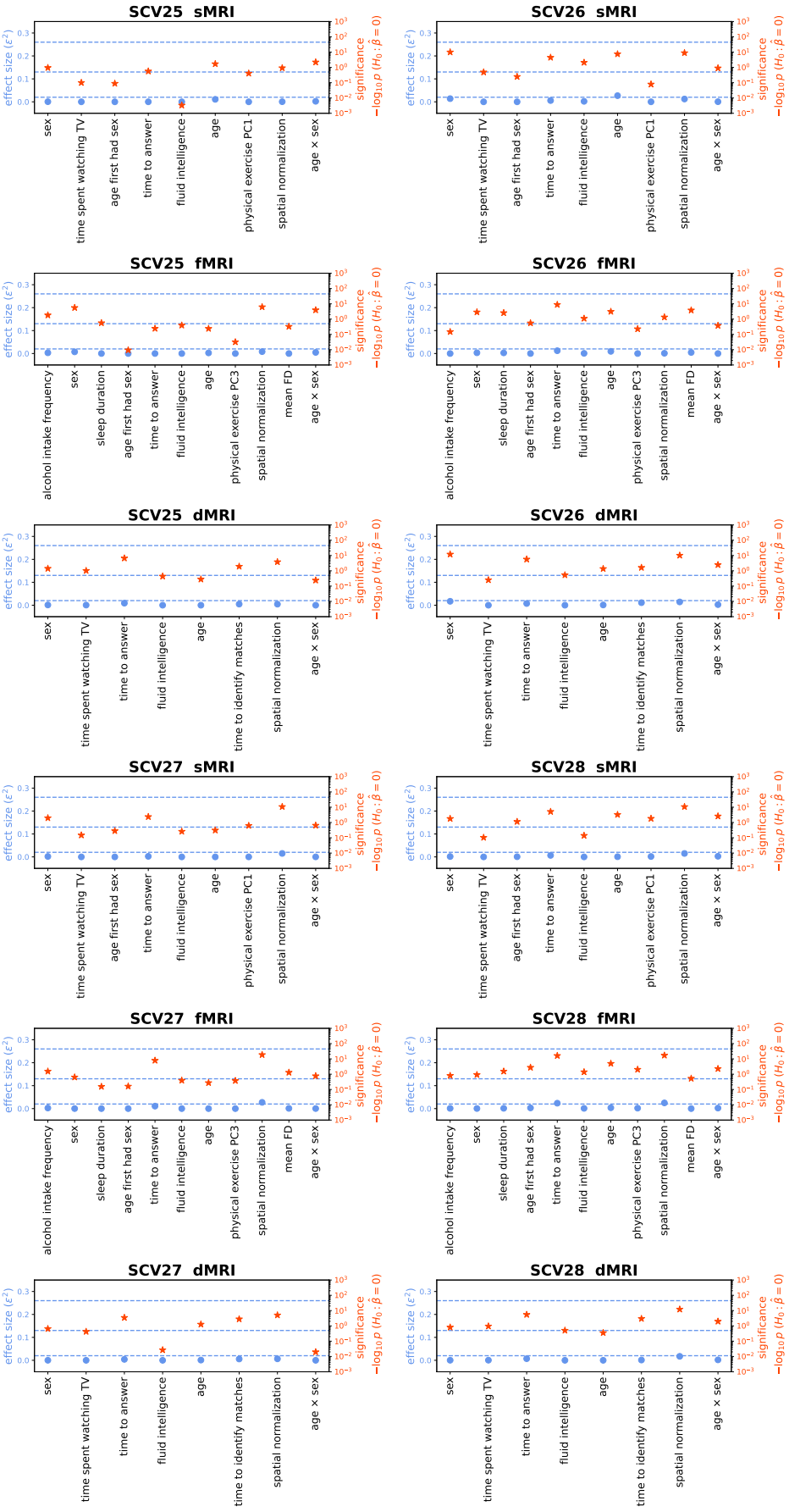
SCV25 sMRI
SCV26 sMRI
SCV25 fMRI
SCV26 fMRI
SCV25 dMRI
SCV26 dMRI
SCV27 sMRI
SCV28 sMRI
SCV27 fMRI
SCV28 fMRI
SCV27 dMRI
SCV28 dMRI
effect size (ε^2)
significance
$-\log_{10} p\ (H_0 : \hat{\beta} = 0)$
sex
time spent watching TV
age first had sex
time to answer
fluid intelligence
age
physical exercise PC1
spatial normalization
age × sex
alcohol intake frequency
sleep duration
physical exercise PC3
mean FD
time to identify matches

(g) SCVs 25-28

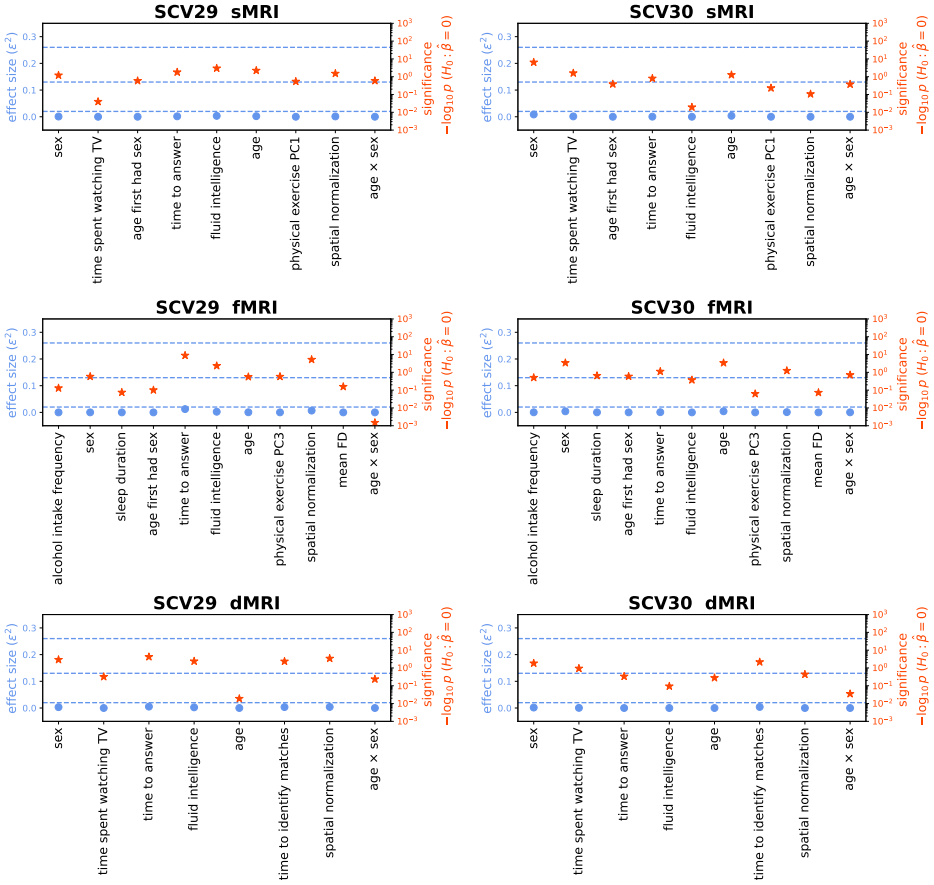

(h) SCVs 29-30

Figure S8: **Effect Size Measure (UK Biobank Dataset).** Red star indicates significance level, while blue dot indicates effect size. Blue horizontal dashed lines from bottom to top indicate thresholds for small ($\epsilon^2 = 0.02$), medium ($\epsilon^2 = 0.13$), and large ($\epsilon^2 = 0.26$) effect sizes, respectively.

S1.9. Effect Size Measure (Patient Dataset)

For the patient dataset, we fit linear models using the same 7 variables (age, sex, diagnosis, the interaction between age and sex, the interaction between age and diagnosis, the interaction between sex and diagnosis, the interaction among age, sex and diagnosis) to predict unimodal sources in each of the three modalities, with 2 additional variables (spatial normalization and mean framewise displacement) included for fMRI.

For a categorical variable with more than two categories, such as diagnosis with six categories, we fit another linear regression model without the categorical variable and its interaction(s), namely a reduced model. We obtained the statistics of the categorical variable from the ANOVA analysis between the reduced model and full model.

No interaction terms were significant, so only Type II effect sizes are reported (except for dMRI of SCV 5).

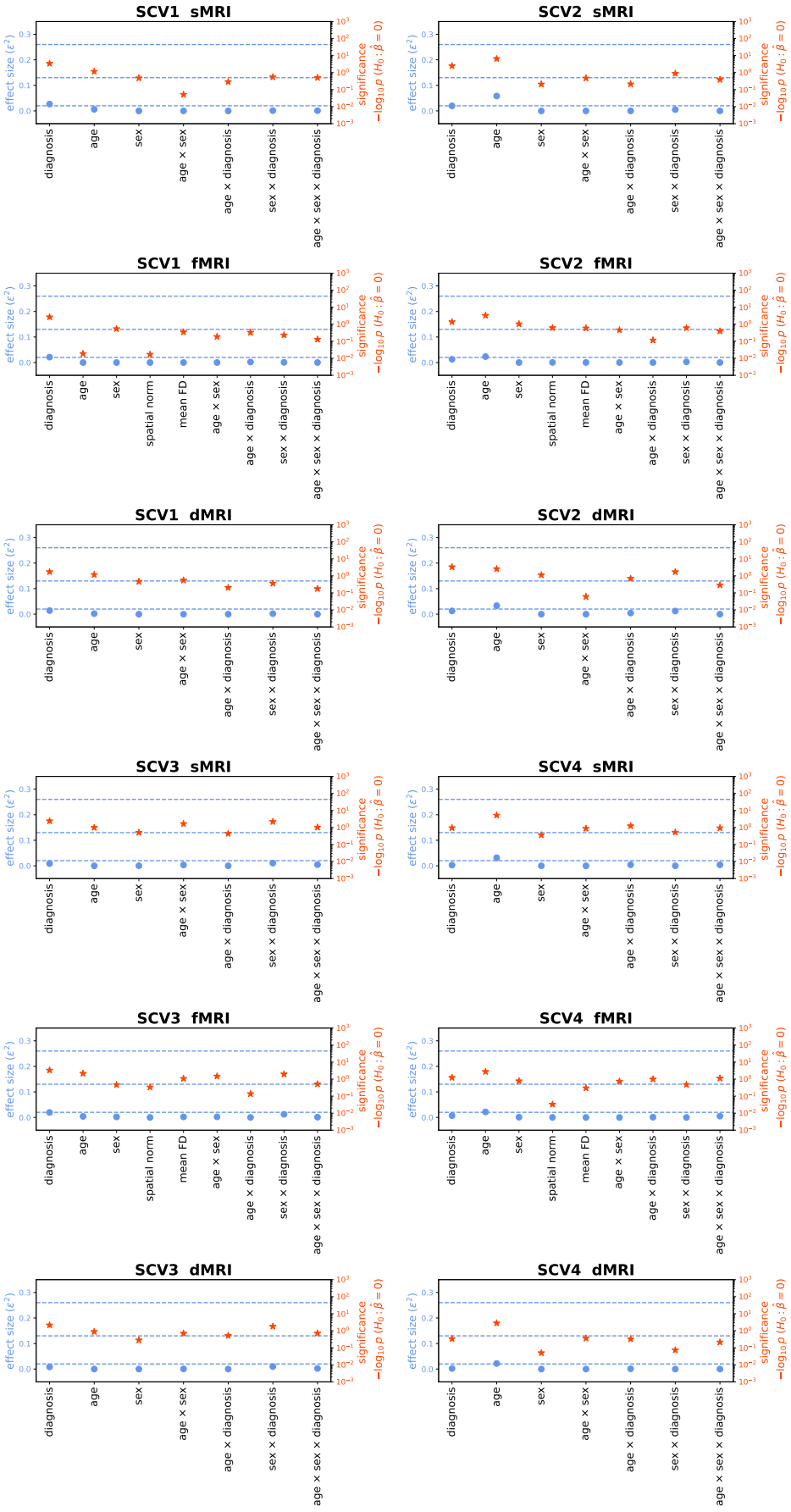
SCV1 sMRI
SCV2 sMRI
SCV1 fMRI
SCV2 fMRI
SCV1 dMRI
SCV2 dMRI
SCV3 sMRI
SCV4 sMRI
SCV3 fMRI
SCV4 fMRI
SCV3 dMRI
SCV4 dMRI
effect size (ε^2)
significance
$-\log_{10} p\ (H_0 : \hat{\beta} = 0)$
diagnosis
age
sex
spatial norm
mean FD
age × sex
age × diagnosis
sex × diagnosis
age × sex × diagnosis

(a) SCVs 1-4

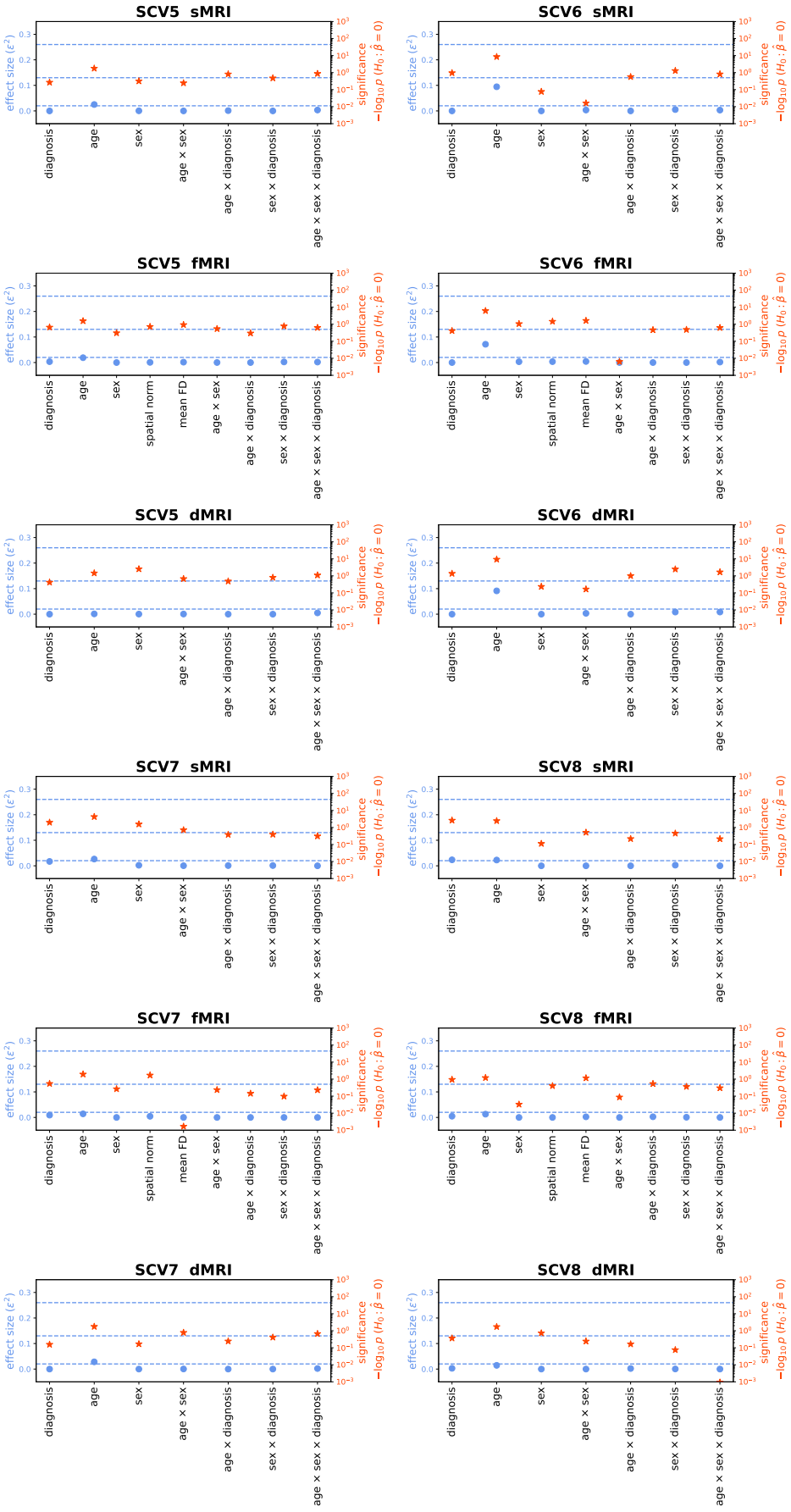
SCV5 sMRI
SCV6 sMRI
SCV5 fMRI
SCV6 fMRI
SCV5 dMRI
SCV6 dMRI
SCV7 sMRI
SCV8 sMRI
SCV7 fMRI
SCV8 fMRI
SCV7 dMRI
SCV8 dMRI
effect size (ε^2)
significance
$-\log_{10} p\ (H_0 : \hat{\beta} = 0)$
diagnosis
age
sex
spatial norm
mean FD
age × sex
age × diagnosis
sex × diagnosis
age × sex × diagnosis

(b) SCVs 5-8

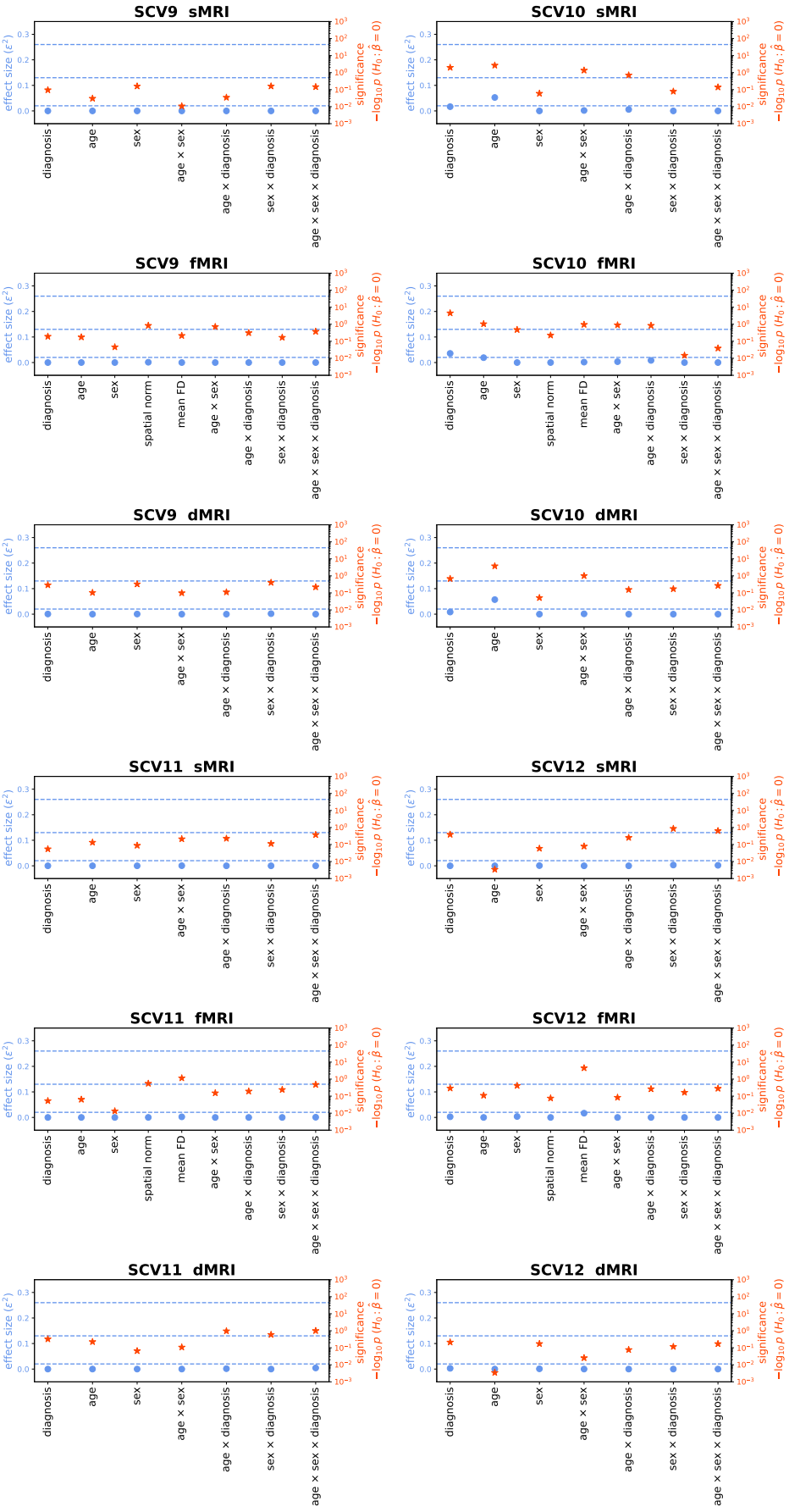
SCV9 sMRI
SCV10 sMRI
SCV9 fMRI
SCV10 fMRI
SCV9 dMRI
SCV10 dMRI
SCV11 sMRI
SCV12 sMRI
SCV11 fMRI
SCV12 fMRI
SCV11 dMRI
SCV12 dMRI
effect size (ε^2)
significance
$-\log_{10} p\ (H_0 : \hat{\beta} = 0)$
diagnosis
age
sex
spatial norm
mean FD
age × sex
age × diagnosis
sex × diagnosis
age × sex × diagnosis

(c) SCVs 9-12

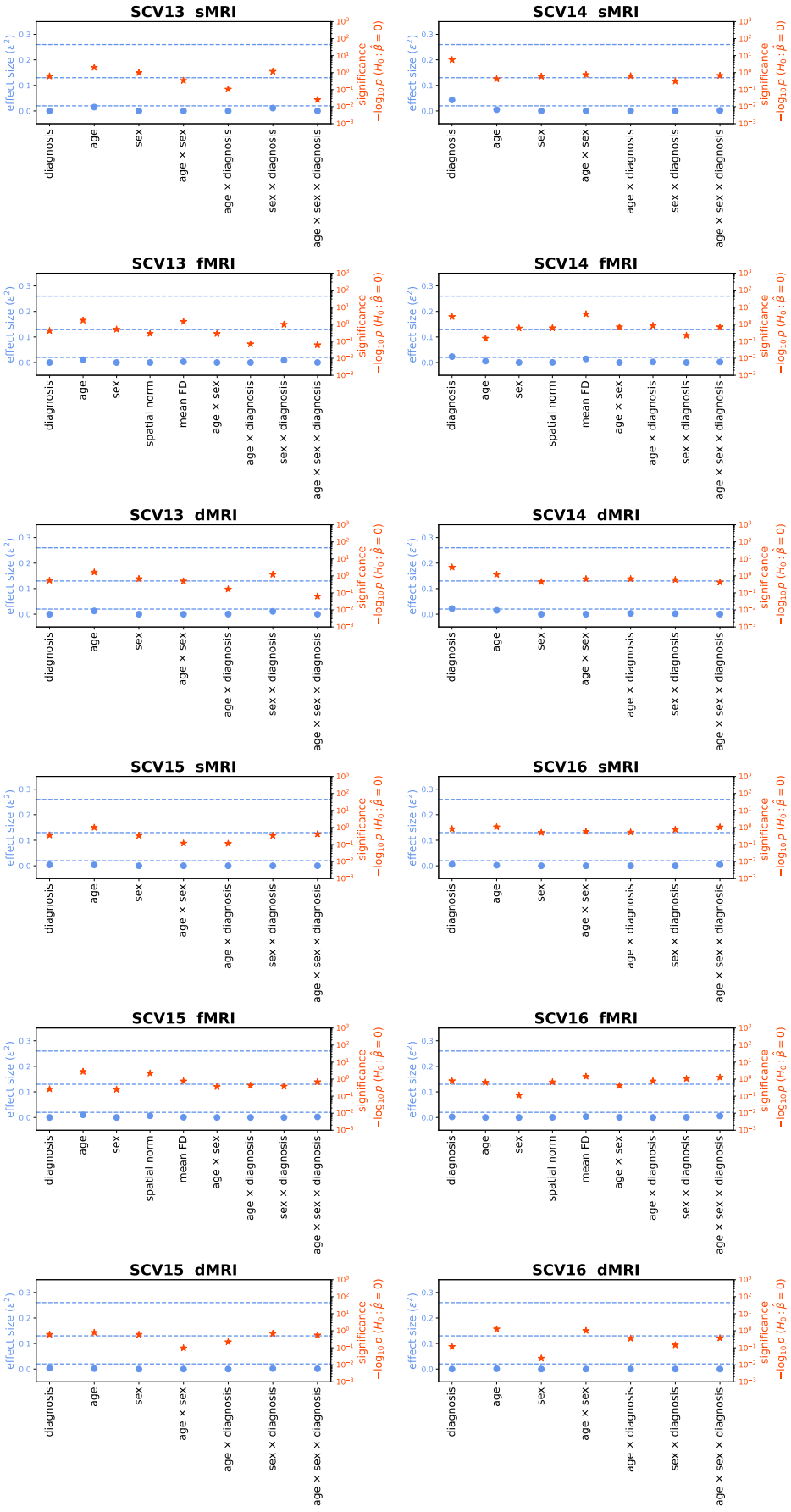
SCV13 sMRI
SCV14 sMRI
SCV13 fMRI
SCV14 fMRI
SCV13 dMRI
SCV14 dMRI
SCV15 sMRI
SCV16 sMRI
SCV15 fMRI
SCV16 fMRI
SCV15 dMRI
SCV16 dMRI
effect size (ε^2)
significance
$-\log_{10} p\ (H_0 : \hat{\beta} = 0)$
diagnosis
age
sex
spatial norm
mean FD
age × sex
age × diagnosis
sex × diagnosis
age × sex × diagnosis

(d) SCVs 13-16

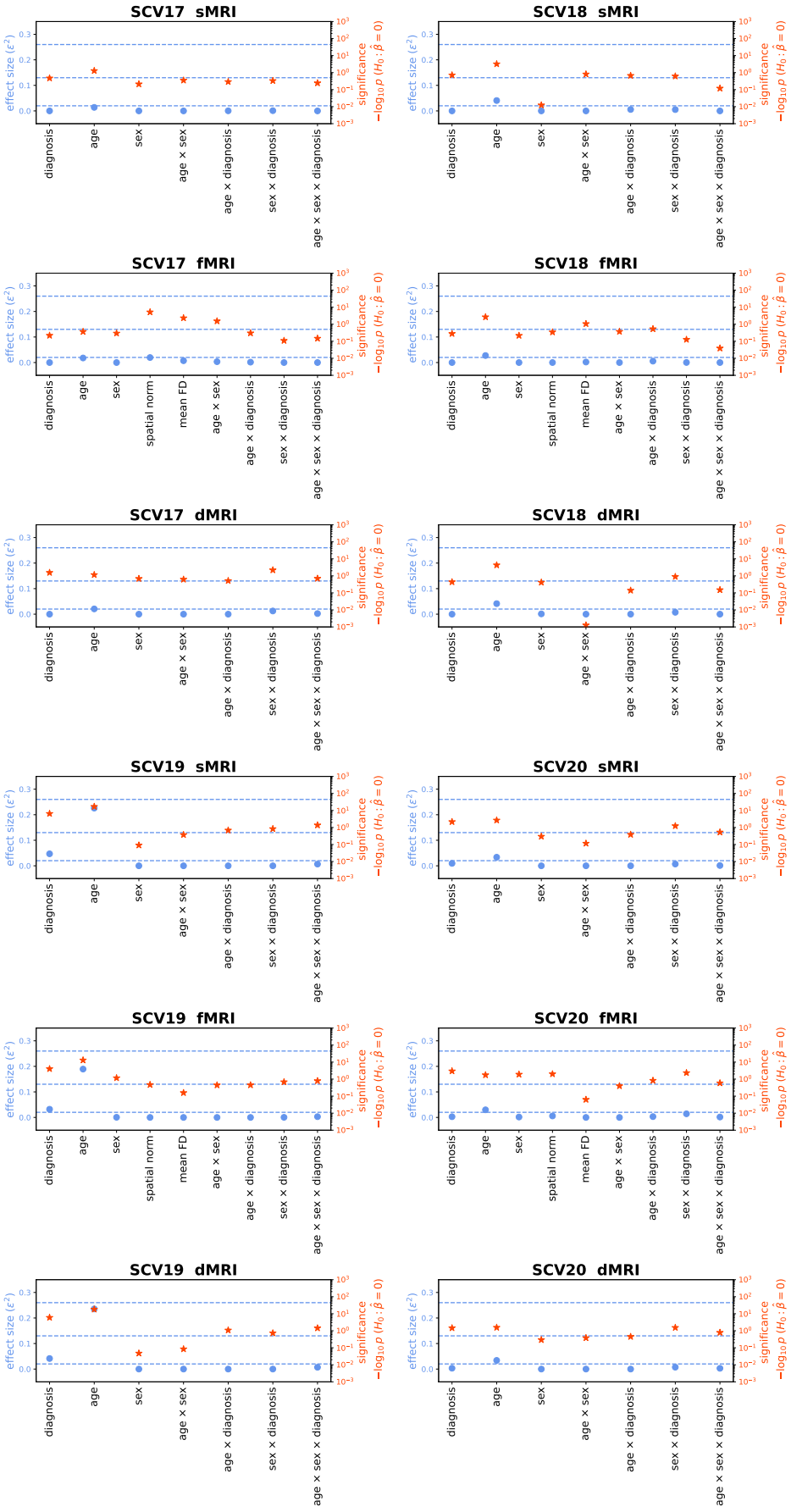
SCV17 sMRI
SCV18 sMRI
SCV17 fMRI
SCV18 fMRI
SCV17 dMRI
SCV18 dMRI
SCV19 sMRI
SCV20 sMRI
SCV19 fMRI
SCV20 fMRI
SCV19 dMRI
SCV20 dMRI
effect size (ε^2)
significance
$-\log_{10} p\ (H_0 : \hat{\beta} = 0)$
diagnosis
age
sex
spatial norm
mean FD
age × sex
age × diagnosis
sex × diagnosis
age × sex × diagnosis

(e) SCVs 17-20

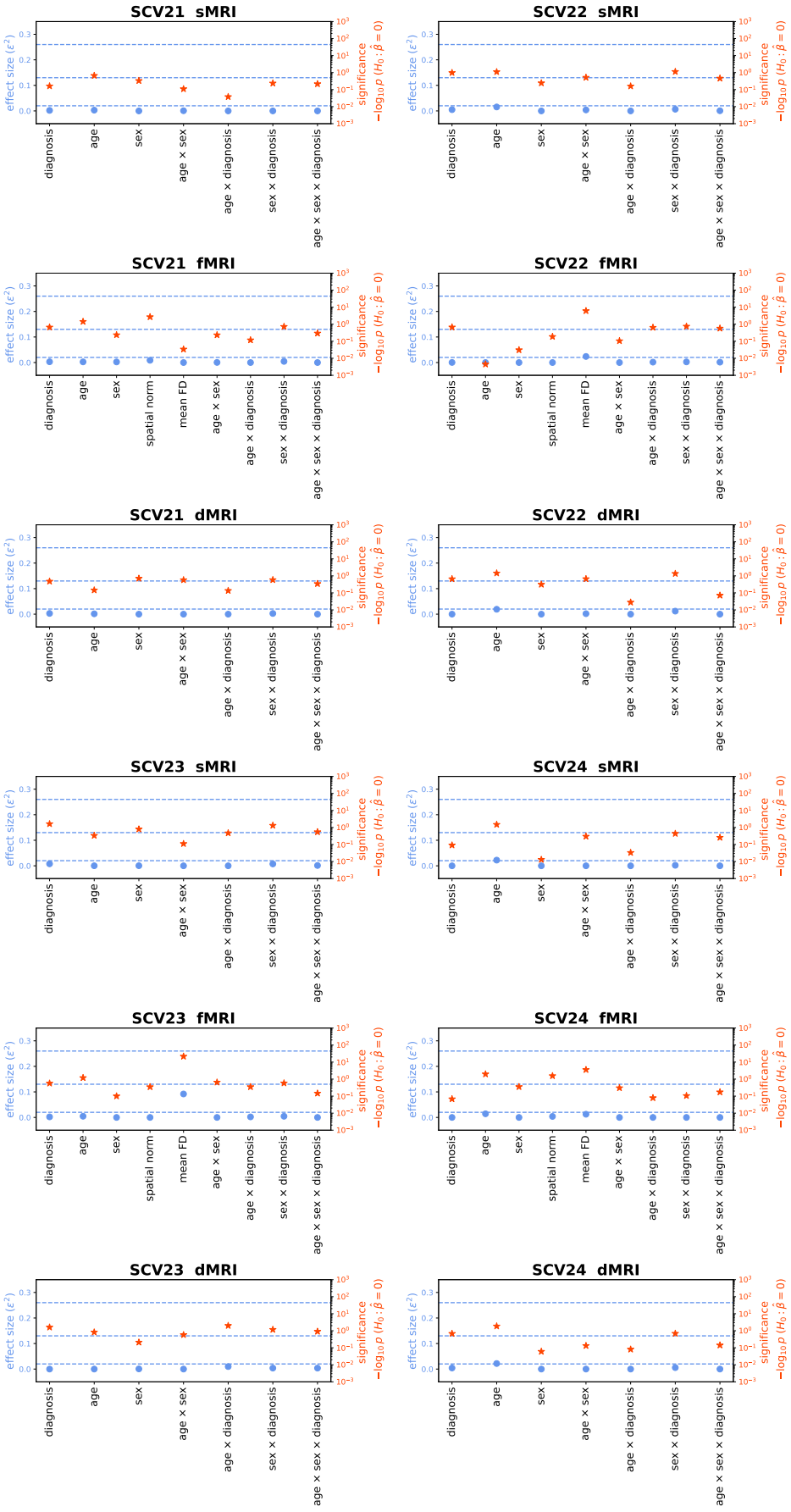
SCV21 sMRI
SCV22 sMRI
SCV21 fMRI
SCV22 fMRI
SCV21 dMRI
SCV22 dMRI
SCV23 sMRI
SCV24 sMRI
SCV23 fMRI
SCV24 fMRI
SCV23 dMRI
SCV24 dMRI
effect size (ε^2)
significance
$-\log_{10} p\ (H_0 : \hat{\beta} = 0)$
diagnosis
age
sex
spatial norm
mean FD
age × sex
age × diagnosis
sex × diagnosis
age × sex × diagnosis

(f) SCVs 21-24

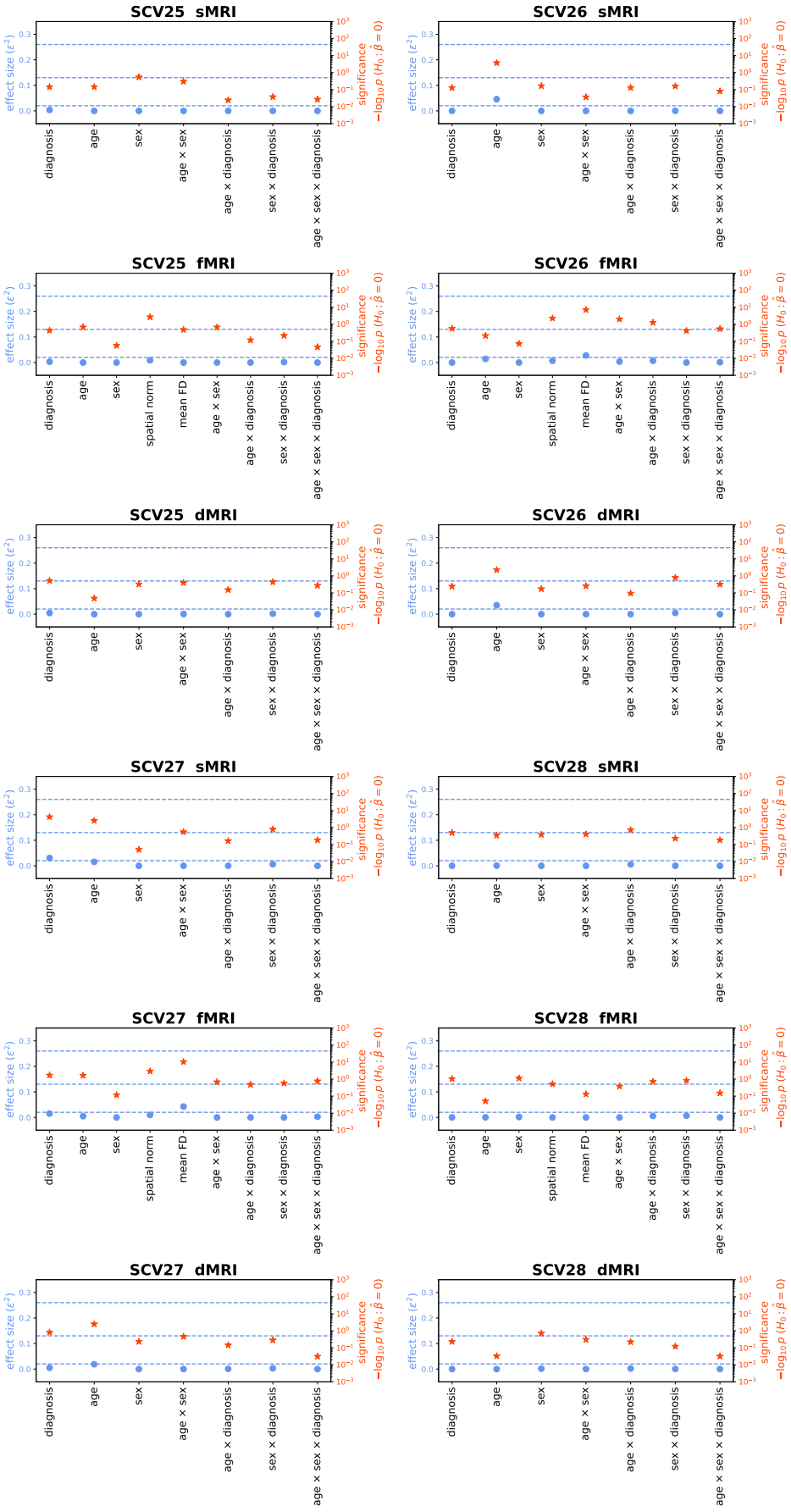
SCV25 sMRI
SCV26 sMRI
SCV25 fMRI
SCV26 fMRI
SCV25 dMRI
SCV26 dMRI
SCV27 sMRI
SCV28 sMRI
SCV27 fMRI
SCV28 fMRI
SCV27 dMRI
SCV28 dMRI
effect size (ε^2)
significance
$-\log_{10} p\ (H_0 : \hat{\beta} = 0)$
diagnosis
age
sex
spatial norm
mean FD
age × sex
age × diagnosis
sex × diagnosis
age × sex × diagnosis

(g) SCVs 25-28

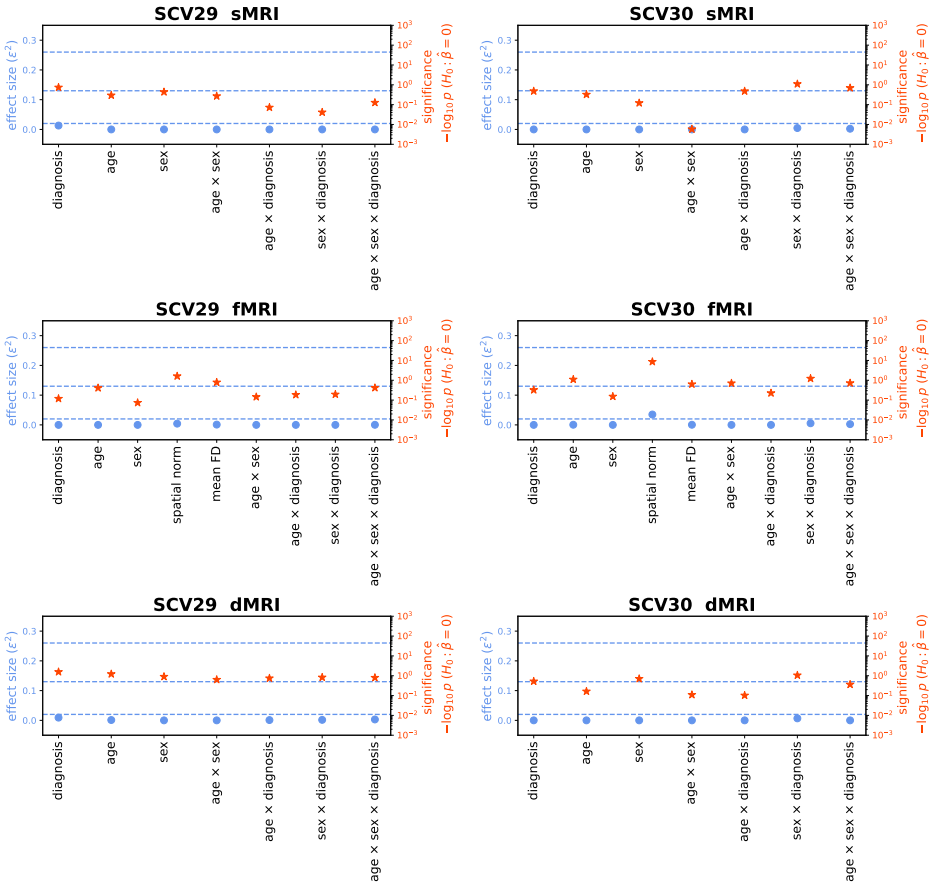

(h) SCVs 29-30

Figure S9: **Effect Size Measure (Patient Dataset).** Red star indicates significance level, while blue dot indicates effect size. Blue horizontal dashed lines from bottom to top indicate thresholds for small ($\epsilon^2 = 0.02$), medium ($\epsilon^2 = 0.13$), and large ($\epsilon^2 = 0.26$) effect sizes, respectively.

References

Alfaro-Almagro, F., Jenkinson, M., Bangerter, N. K., Andersson, J. L., Griffanti, L., Douaud, G., Sotiropoulos, S. N., Jbabdi, S., Hernandez-Fernandez, M., Vallee, E., et al., 2018. Image processing and quality control for the first 10,000 brain imaging datasets from uk biobank. Neuroimage 166, 400–424.

Caprihan, A., Abbott, C., Yamamoto, J., Pearlson, G., Perrone-Bizzozero, N., Sui, J., Calhoun, V. D., 2011. Source-Based Morphometry Analysis of Group Differences in Fractional Anisotropy in Schizophrenia. Brain Connect 1 (2), 133–145.

Cetin-Karayumak, S., Di Biase, M. A., Chunga, N., Reid, B., Somes, N., Lyall, A. E., Kelly, S., Solgun, B., Pasternak, O., Vangel, M., Pearlson, G., Tamminga, C., Sweeney, J. A., Clementz, B., Schretlen, D., Viher, P. V., Stegmayer, K., Walther, S., Lee, J., Crow, T., James, A., Voineskos, A., Buchanan, R. W., Szeszko, P. R., Malhotra, A. K., Hegde, R., McCarley, R., Keshavan, M., Shenton, M., Rathi, Y., Kubicki, M., 2020. White matter abnormalities across the lifespan of schizophrenia: a harmonized multi-site diffusion MRI study. Mol Psychiatry 25 (12), 3208–3219.

Giakoumatos, C., Nanda, P., Mathew, I., Tandon, N., Shah, J., Bishop, J., Clementz, B., Pearlson, G., Sweeney, J., Tamminga, C., Keshavan, M., 2015. Effects of lithium on cortical thickness and hippocampal subfield volumes in psychotic bipolar disorder. Journal of Psychiatric Research 61, 180–187.

Griffanti, L., Salimi-Khorshidi, G., Beckmann, C. F., Auerbach, E. J., Douaud, G., Sexton, C. E., Zsoldos, E., Ebmeier, K. P., Filippini, N., Mackay, C. E., et al., 2014. Ica-based artefact removal and accelerated fmri acquisition for improved resting state network imaging. Neuroimage 95, 232–247.

Herskovits, E. H., Hong, L. E., Kochunov, P., Sampath, H., Chen, R., 2015. Edge-Centered DTI Connectivity Analysis: Application to Schizophrenia. Neuroinform 13 (4), 501–509.

INDI, 2022. Retrospective Data Sharing Samples.
URL http://fcon_1000.projects.nitrc.org/indi/retro/cobre.html

Qi, S., Calhoun, V. D., van Erp, T. G. M., Bustillo, J., Damaraju, E., Turner, J. A., Du, Y., Yang, J., Chen, J., Yu, Q., Mathalon, D. H., Ford, J. M., Voyvodic, J., Mueller, B. A., Belger, A., McEwen, S., Potkin, S. G., Preda, A., Jiang, T., Sui, J., 2018. Multimodal Fusion With Reference: Searching for Joint Neuromarkers of Working Memory Deficits in Schizophrenia. IEEE Trans. Med. Imaging 37 (1), 93–105.

Qi, S., Sui, J., Pearlson, G., Bustillo, J., Perrone-Bizzozero, N. I., Kochunov, P., Turner, J. A., Fu, Z., Shao, W., Jiang, R., Yang, X., Liu, J., Du, Y., Chen, J., Zhang, D., Calhoun, V. D., 2022. Derivation and utility of schizophrenia polygenic risk associated multimodal MRI frontotemporal network. Nat Commun 13 (1), 4929.

Schijven, D., Postema, M. C., Fukunaga, M., Matsumoto, J., Miura, K., de Zwarte, S. M. C., van Haren, N. E. M., Cahn, W., Hulshoff Pol, H. E., Kahn, R. S., Ayesa-Arriola, R., Ortiz-García de la Foz, V., Tordesillas-Gutierrez, D., Vázquez-Bourgon, J., Crespo-Facorro, B., Alnæs, D., Dahl, A., Westlye, L. T., Agartz, I., Andreassen, O. A., Jönsson, E. G., Kochunov, P., Bruggemann, J. M., Catts, S. V., Michie, P. T., Mowry, B. J., Quidé, Y., Rasser, P. E., Schall, U., Scott, R. J., Carr, V. J., Green, M. J., Henskens, F. A., Loughland, C. M., Pantelis, C., Weickert, C. S., Weickert, T. W., de Haan, L., Brosch, K., Pfarr, J.-K., Ringwald, K. G., Stein, F., Jansen, A., Kircher, T. T. J., Nenadić, I., Krämer, B., Gruber, O., Satterthwaite, T. D., Bustillo, J., Mathalon, D. H., Preda, A., Calhoun, V. D., Ford, J. M., Potkin, S. G., Chen, J., Tan, Y., Wang, Z., Xiang, H., Fan, F., Bernardoni, F., Ehrlich, S., Fuentes-Claramonte, P., Garcia-Leon, M. A., Guerrero-Pedraza, A., Salvador, R., Sarró, S., Pomarol-Clotet, E., Ciullo, V., Piras, F., Vecchio, D., Banaj, N., Spalletta, G., Michielse, S., van Amelsvoort, T., Dickie, E. W., Voineskos, A. N., Sim, K., Ciufolini, S., Dazzan, P., Murray, R. M., Kim, W.-S., Chung, Y.-C., Andreou, C., Schmidt, A., Borgwardt, S., McIntosh, A. M., Whalley, H. C., Lawrie, S. M., du Plessis, S., Luckhoff, H. K., Scheffler, F., Emsley, R., Grotegerd, D., Lencer, R., Dannlowski, U., Edmond, J. T., Rootes-Murdy, K., Stephen, J. M., Mayer, A. R., Antonucci, L. A., Fazio, L., Pergola, G., Bertolino, A., Díaz-Caneja, C. M., Janssen, J., Lois, N. G., Arango, C., Tomyshev, A. S., Lebedeva, I., Cervenka, S., Sellgren, C. M., Georgiadis, F., Kirschner, M., Kaiser, S., Hajek, T., Skoch, A., Spaniel, F., Kim, M., Kwak, Y. B., Oh, S., Kwon, J. S., James, A., Bakker, G., Knöchel, C., Stäblein, M., Oertel, V., Uhlmann, A., Howells, F. M., Stein, D. J., Temmingh, H. S., Diaz-Zuluaga, A. M., Pineda-Zapata, J. A., López-Jaramillo, C., Homan, S., Ji, E., Surbeck, W., Homan, P., Fisher, S. E., Franke, B., Glahn, D. C., Gur, R. C., Hashimoto, R., Jahanshad, N., Luders, E., Medland, S. E., Thompson, P. M., Turner, J. A., van Erp, T. G. M., Francks, C., 2023. Large-scale analysis of structural brain asymmetries in schizophrenia via the ENIGMA consortium. Proceedings of the National Academy of Sciences 120 (14), e2213880120.

Wang, Q., Chen, R., JaJa, J., Jin, Y., Hong, L. E., Herskovits, E. H., 2016. Connectivity-Based Brain Parcellation: A Connectivity-Based Atlas for Schizophrenia Research. Neuroinform 14 (1), 83–97.

Wright, S. N., Hong, L. E., Winkler, A. M., Chiappelli, J., Nugent, K., Muellerklein, F., Du, X., Rowland, L. M., Wang, D. J. J., Kochunov, P., 2015. Perfusion shift from white to gray matter may account for processing speed deficits in schizophrenia: Perfusion Shift from White to Gray Matter. Hum. Brain Mapp. 36 (10), 3793–3804.

Wu, L., Calhoun, V. D., Jung, R. E., Caprihan, A., 2015. Connectivity-based whole brain dual parcellation by group ICA reveals tract structures and decreased connectivity in schizophrenia. Hum Brain Mapp 36 (11), 4681–4701.

Zhao, N., Yuan, L.-X., Jia, X.-Z., Zhou, X.-F., Deng, X.-P., He, H.-J., Zhong, J., Wang, J., Zang, Y.-F., 2018. Intra-and inter-scanner reliability of voxel-wise whole-brain analytic metrics for resting state fmri. Frontiers in neuroinformatics 12, 54.